71-4673

MARSHAK, Marvin Lloyd, 1946-
PROTON-NEUTRON ELASTIC SCATTERING FROM DEUTERIUM.

The University of Michigan, Ph.D., 1970
Physics, elementary particles

University Microfilms, A XEROX Company, Ann Arbor, Michigan

PROTON-NEUTRON ELASTIC SCATTERING FROM DEUTERIUM

by

Marvin Lloyd Marshak

A dissertation submitted in partial fulfillment
of the requirements for the degree of
Doctor of Philosophy in
The University of Michigan
1970

Doctoral Committee:

Professor Alan D. Krisch, Chairman
Assistant Professor Charles R. Cowley
Professor Oliver E. Overseth
Professor Marc H. Ross

PREFACE

One may quite reasonably inquire why the experiment described here was done. An almost sufficient answer is that it had never been done before. That reason alone has certainly led men to perform many deeds. But there are additional justifications for this particular experiment. It touches one one of the most basic and most aesthetically pleasing principles in physics and perhaps knowledge in general--the idea of symmetry. In physics symmetry principles have led to such general laws as the conservation of momentum and energy and the conservation of angular momentum. Symmetry has played an important role in some of the most exciting discoveries of elementary particle physics--the production of anti-matter, the eight-fold way and the Ω^- hyperon, and CP violation in K^o meson decay. Much yet needs to be understood about such symmetries, including one which has been known for several decades--the nucleon system. The proton and neutron are alike in many respects--baryon number, strangeness, spin, total isospin and near equality of mass. They differ in charge or the z component of isospin. Is that the only difference? Do they behave differently in strong interactions? Why is the charged nucleon lighter when it would seem to have more "self energy"?

How does one answer these questions? The best known probe into the inner structure of particles is scattering

processes. The structural resolution obtained by scattering reactions depends on the momentum transferred to the scattered particle. Unfortunately, as this momentum transfer increases, the probability of a scattering decreases exponentially. The proton has been probed to a resolution of 3×10^{-14} cm revealing surprising structure of this incredibly small size; present experimental technique has limited experimenters seeking to delve into the inside of the neutron to structures several times larger. The state of present knowledge is limited, but to the accuracy currently obtainable, they seem very similar. But why then two symmetric states of the nucleon? Is there some inner difference yet to be discovered?

This experiment seeks to develop a new technique to permit finer and more accurate probing of the structure of the neutron. To the extent that it has been successful, it will permit future experiments to seek more information about the relationship of neutrons and protons.

ACKNOWLEDGEMENTS

I have been truly fortunate in my brief tenure at the University of Michigan to have had the opportunity to associate with so many people who have made significant contributions to my development as a physicist and as a person. I perform the usual injustice by acknowledging the assistance of some and ignoring that of others, but I do so in the certainty that those whom I do and do not mention are all deserving of my thanks.

Alan Krisch--who taught me much of what I know about elementary particle physics in such a way that I will not easily forget what I have learned. Although at times I may have disagreed with his means, I reject not at all the final effect.

Larry Ratner--who provided compassion and understanding without which I could not have done any learning.

Peter Schmüser--who exposed me to a different point of view and challenged me to use my judgment to decide between them.

Marc Ross and Gordy Kane--who encouraged an appreciation of a more global attitude towards physics and society.

John Day, Kemp Randolph and Gerry Bunce--who provided companionship to discuss both physics and any other subject known to man.

My parents, Kalman and Goldie Marshak--whose beneficial influence began long before I came to Ann Arbor and will continue long after I leave; whose sustenance, both tangible

and intangible, has allowed me to reach this point in my life.

I also acknowledge the assistance of the entire staff of the Argonne ZGS in executing the experiment described here and the support of this research by the U. S. Atomic Energy Commission.

TABLE OF CONTENTS

	Page
PREFACE	ii
ACKNOWLEDGEMENTS	iv
LIST OF FIGURES	vii
LIST OF TABLES	vii
I. Introduction	1
II. Experimental Method	5
A. Proton Beam and Monitoring	5
B. Deuterium Target	9
C. Spectrometer and Counters	11
D. The Sandwich Counter	12
E. Electronics	21
III. Results	27
A. Corrections and Experimental Errors	27
B. Proton-Proton Scattering	32
C. Proton-Neutron Scattering	33
IV. Discussion	35
A. Multiple Scattering	35
B. Neutron-Proton Elastic Scattering	37
C. The Deuterium Target Technique	39
REFERENCES	44
APPENDIX	47
A. The Sandwich Counter	48
B. The Monte Carlo Simulation	50
C. Results	54
D. Conclusions	60
REFERENCES (in the Appendix)	61

LIST OF FIGURES

Figure		Page
1.	Experimental Layout	6
2.	Sandwich Counter	7
3.	Deuterium Target	10
4.	Longitudinal Development of Nuclear Cascade	16
5.	Proton and Neutron Efficiencies	17
6.	Neutron Efficiency and Distribution	19
7.	Proton Efficiency and Distribution	20
8.	Logic Diagram	23
9.	Time-of-Flight Spectrum	26
10.	PP Elastic Scattering Peak	29
11.	Quasi-Elastic Scattering Peak	30
12.	Proton-Neutron Elastic Scattering	38
13.	Detection Efficiency Profile	56
14.	Efficiency as Function of Incident Momentum	58

LIST OF TABLES

Table		Page
1.	Corrections and Errors	28

I. INTRODUCTION

The structure observed in proton-proton elastic scattering makes the isospin related neutron-proton elastic scattering a process of considerable interest. For experimental reasons, the np elastic cross-section has not been measured over nearly the same range of four-momentum transfers or with the same accuracy as the pp cross-section. Experimental technique has allowed reliable measurements of proton-proton cross-sections[1] as small as 10^{-36} cm^2/sr corresponding to $t = -20$ $(GeV/c)^2$. It has not yet been possible to measure np cross-sections[2] less than 10^{-30} cm^2/sr with comparable accuracy.

The difficulties encountered in previous pn elastic scattering experiments are not very tractable since they arise from the characteristics of the incident neutron beam. 1) The intensity of a produced neutron beam is approximately a factor of a million less than the intensity of the primary proton beam. 2) The absolute intensity of the neutron beam cannot be easily measured; the observed differential cross-sections are usually normalized to the optical point. This procedure results in a normalization uncertainty from the imprecise knowledge of the phase of the scattering amplitude. 3) The momentum spectrum of the neutron beam is broad and can only be inferred from the analysis of scattering events; the necessity for reconstructing the incident momentum places tight demands on the resolution of detection of the outgoing particles.

In response to these deficiencies, we measured the pn elastic cross-section using a proton beam and a deuterium target. This method solves all the problems of the neutron beam experiment since the proton beam has a high intensity, can be normalized by foil spallation techniques within seven percent and is monochromatic to one-half percent. However, the extraction of the free nucleon-nucleon cross-section from the resultant raw data is complicated by several effects. 1) The Fermi momentum of the bound nucleons in the target deuteron smears the momentum and angular distributions of the scattered particles. Discrimination between elastic and inelastic events and double-arm detection of all elastic events become difficult. 2) Multiple scattering or screening effects in the target deuteron affect the measured cross-section. 3) Accurate quantitative results require the detection of the recoil nucleon with well-calibrated efficiency. A subsidiary problem is that the high background flux near an intense proton beam may swamp the large volume counter required to detect a reasonable percentage of the recoil neutrons.

In order to correct for the first two effects, we simultaneously measured pp and pn elastic scattering from deuterium as well as pp scattering from hydrogen. The Fermi momentum effect is certainly identical for pp and pn scattering and drops out of a ratio of

$$R = \frac{\left(\frac{d\sigma}{d\Omega}\right)_{pn}}{\left(\frac{d\sigma}{d\Omega}\right)_{pp}} \qquad (1)$$

The detection of both the forward proton and the recoil nucleon in coincidence limits the types of multiple scattering processes that can occur. The primary scattering must be at approximately the full momentum transfer and any scattering on the "spectator" nucleon must be at approximately zero momentum transfer in order to satisfy the kinematic requirements placed on the scattered particles. Thus only the scattering amplitudes at zero momentum transfer and the full momentum transfer are relevant. Since the forward pp and pn scattering amplitudes are approximately equal at high energies[3], a consistency argument could indicate that the multiple scattering correction also drops out of the cross-section ratio: assume a priori that the multiple scattering correction is isospin-independent; if the resultant cross-section is the same for pp and pn scattering, then the multiple scattering correction should also be the same. In any event if the multiple scattering defect is a small percentage of the cross-section, then any reasonable isotopic spin dependence should have a second order effect on the cross-section ratio. Thus the free pn elastic cross-section may be determined from the deuterium cross-sections by the equation

$$\left(\frac{d\sigma}{d\Omega}\right)_{\substack{pn \\ free}} = \frac{\left(\frac{d\sigma}{d\Omega}\right)_{pn\ D_2}}{\left(\frac{d\sigma}{d\Omega}\right)_{pp\ D_2}} \left(\frac{d\sigma}{d\Omega}\right)_{\substack{pp \\ free}} \qquad (2)$$

These ideas seem to indicate that the problems associated with the proton-deuterium method are more tractable than the difficulties encountered with the neutron beam technique. To determine their validity, we conducted a short feasibility test in the second extracted proton beam of the Argonne ZGS using essentially the same apparatus as in a previous experiment[4]. Because of the configuration of the apparatus available, we selected for measurement a test point at p_o = 12.4 GeV/c and θ^* = 37° or t = -2.2 $(GeV/c)^2$. The problem of neutron detection was approached using a steel-scintillator sandwich counter. A series of experimental measurements and Monte Carlo calculations determined the absolute detection efficiency of the counter over its entire sensitive area. The intensity of the incident proton beam was limited to 10^{10} protons/pulse so that the singles rate in the sandwich counter resulted in only a small correction for accidental coincidences.

II. EXPERIMENTAL METHOD

The physical layout of the experiment is shown in Fig. 1. The slow extracted proton beam impinged upon a liquid deuterium target. The forward proton was identified and momentum-analyzed by a 35 m spectrometer composed of scintillation counters, bending magnets and a threshold Cherenkov counter. The recoil nucleon passed through a scintillation counter, which determined whether it was charged, and was then detected in a steel-scintillator sandwich counter, shown in Fig. 2. The sandwich counter was made as large as possible so that the spectrometer basically defined the solid angle. Coincidence between the two arms was the indication of an elastic event. The number of protons incident on the target was measured by two monitor telescopes, which were calibrated by a radio-chemical analysis of a gold foil exposed to the beam.

A. Proton Beam and Monitoring

A portion of the circulating proton beam was extracted from the ZGS main ring using the Piccioni energy-loss extraction system. After bending through four extraction magnets, the beam was focused by two sets of quadrupole doublets and was aimed down the experimental beam line by a 72 in. bending magnet. The upstream doublet consisted of two 36 in. quadrupoles and the downstream doublet was four 18 in. quadrupoles, divided into sets of two with the same focusing properties. The desired currents for both the quadrupoles

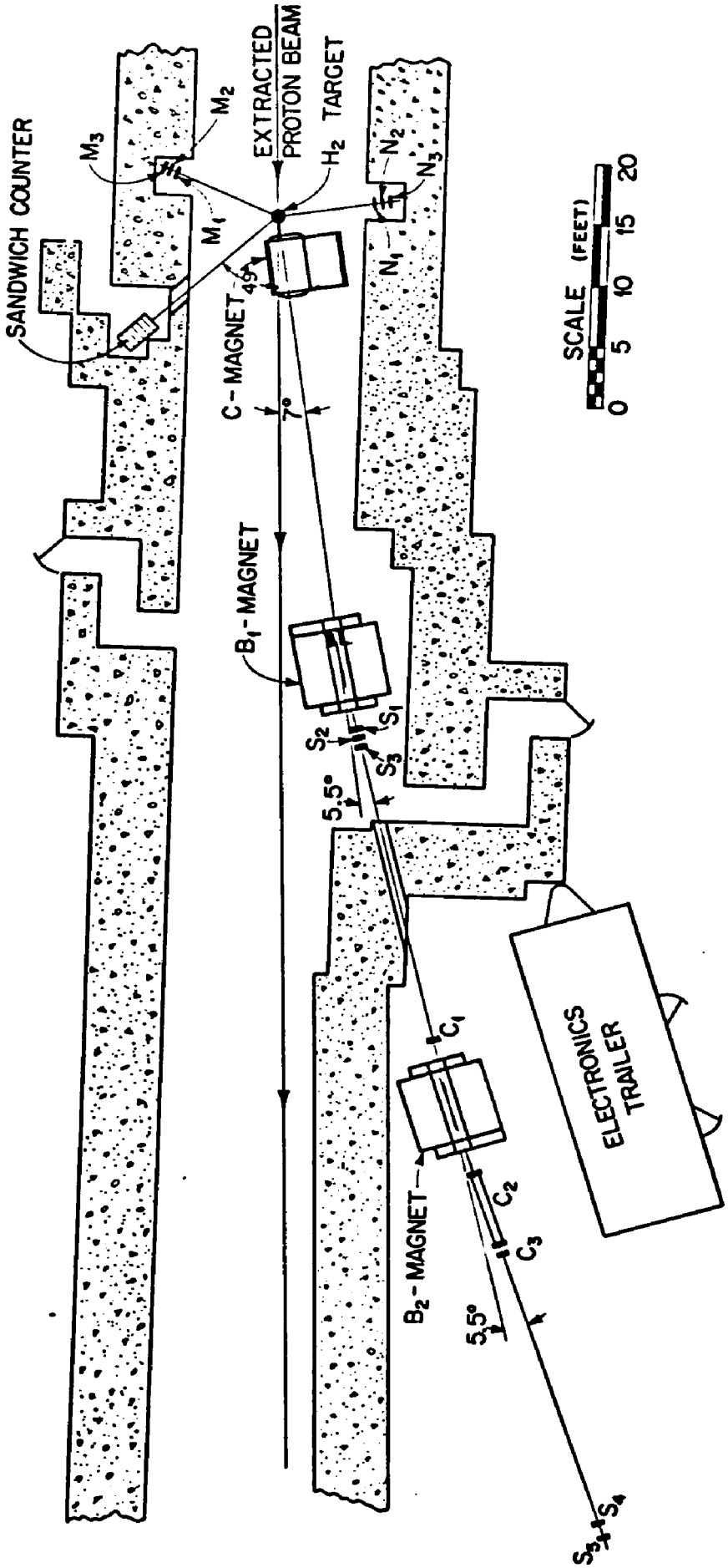

Fig. 1 Experimental layout. The forward proton is detected by the magnetic spectrometer and the recoil nucleon by the sandwich counter.

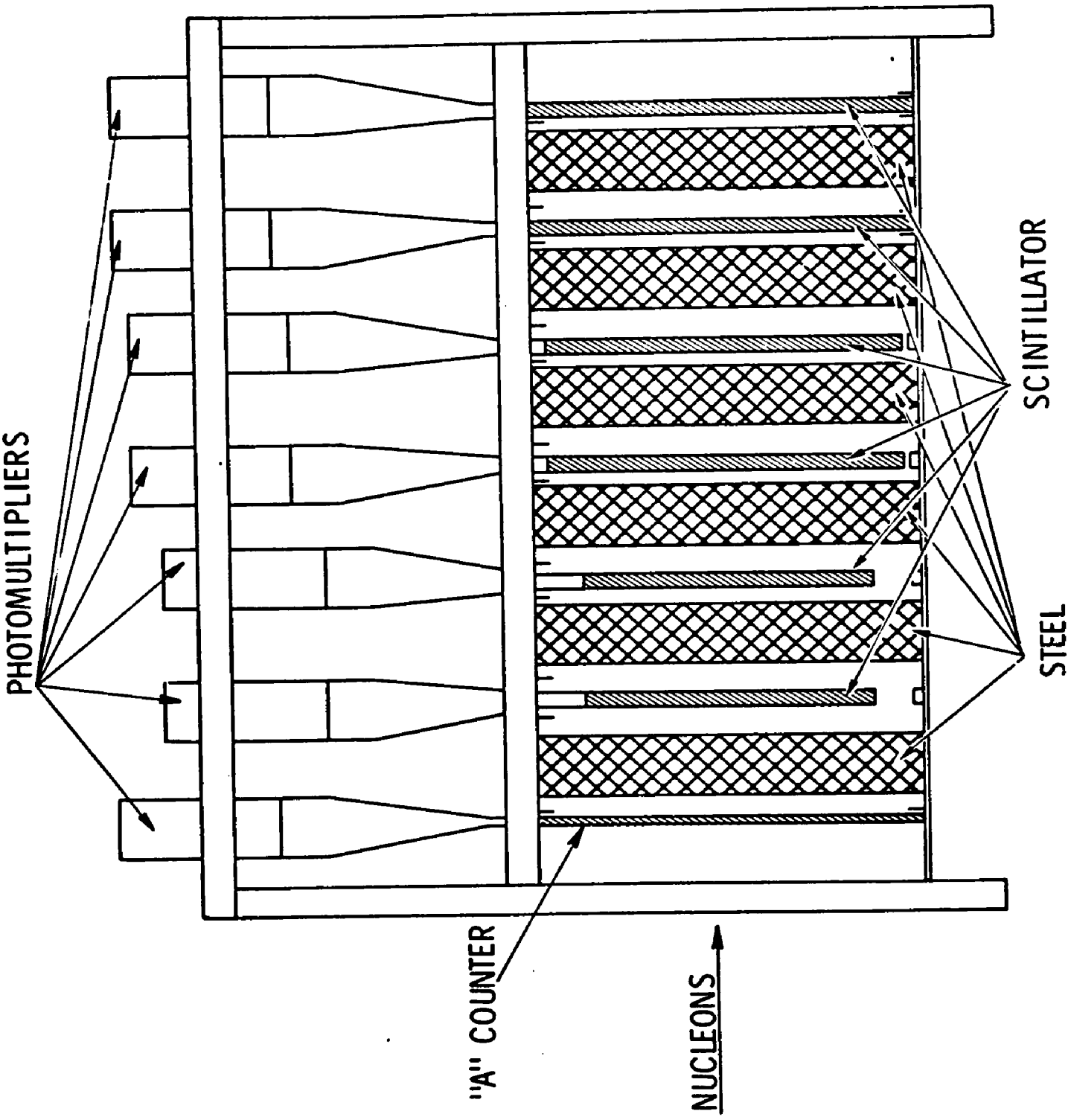

Fig. 2 A side view of the steel-scintillator sandwich counter with the "12 in. total--2 in. between scintillators" steel configuration.

and the bending magnets were computed by standard beam design computer programs. The beam spot size at the target was optimized by replacing the liquid target with a $\frac{1}{4}$ in. square copper target and searching for a maximum number of coincidences in the monitor telescopes as a function of the quadrupole currents.

The tuned beam at the target was $\frac{1}{2}$ in. FWHM both horizontally and vertically. The momentum was 12.4 GeV/c with an absolute uncertainty of $\pm\frac{1}{2}$ percent. The angular divergence was less than 3 millirad FWHM and the monochromaticity was better than $\pm\frac{1}{4}$ percent. The beam intensity was 10^{10} protons per 550 msec spill. The repetition rate was one pulse every 3.3 sec.

The location and size of the proton beam were monitored visually after each ZGS pulse using two devices developed by the ZGS staff. A Segmented Wire Ion Chamber (SWIC)[5] located just upstream of the target displayed the extent of the beam, both horizontally and vertically, on an oscilloscope in the electronics trailer. The output of a Beam Ion Position System (BIPS)[6] detector, placed approximately 15 m downstream of the target, was also located in the trailer. The long lever arm of the BIPS made it quite sensitive to small displacements in the beam position. Straying of the beam as indicated by the BIPS or SWIC was manually corrected by changing the current in the bending magnet in the beam line.

The two monitor telescopes, located just upstream of the target on each side of the tunnel, recorded coincidences in proportion to the number of protons incident on the

target. The monitor counters were $\frac{1}{2}$ x 1 in. Pilot B scintillators; the axis of the three counters pointed to the target through a port in the target casing. The number of events in each telescope was multiplied by a fixed ratio to give each of the two monitor telescopes an approximately equal weight in the determination of the incident intensity. The monitors were normalized to the absolute beam intensity by measuring the characteristic activity of ^{149}Tb produced in a gold foil placed in the beam just upstream of the target during calibration runs. The uncertainty of ±5 percent in the 1.05 mb spallation cross-section for $^{197}Au \rightarrow {}^{149}Tb$ introduced a normalization error in the pp cross-section but did not affect the pp elastic to pn elastic ratio.

B. Deuterium Target

The liquid deuterium target, shown in Fig. 3, was a cylinder about a vertical axis, three inches in diameter. The target was self-refrigerating; an ADL cryostat produced liquid helium which cooled deuterium gas below its boiling point of 21° K. The amount of liquid in the target vessel was indicated by two thermistors, one located at the bottom and the other at the top.

The target flask was 0.003 in. H-film wrapped with several layers of 0.00025 in. aluminized mylar superinsulation. A small hole cut in the mylar allowed a visual check of the liquid level. The target vacuum casing was an aluminum cylinder with 0.322 in. thick walls oriented about the beam

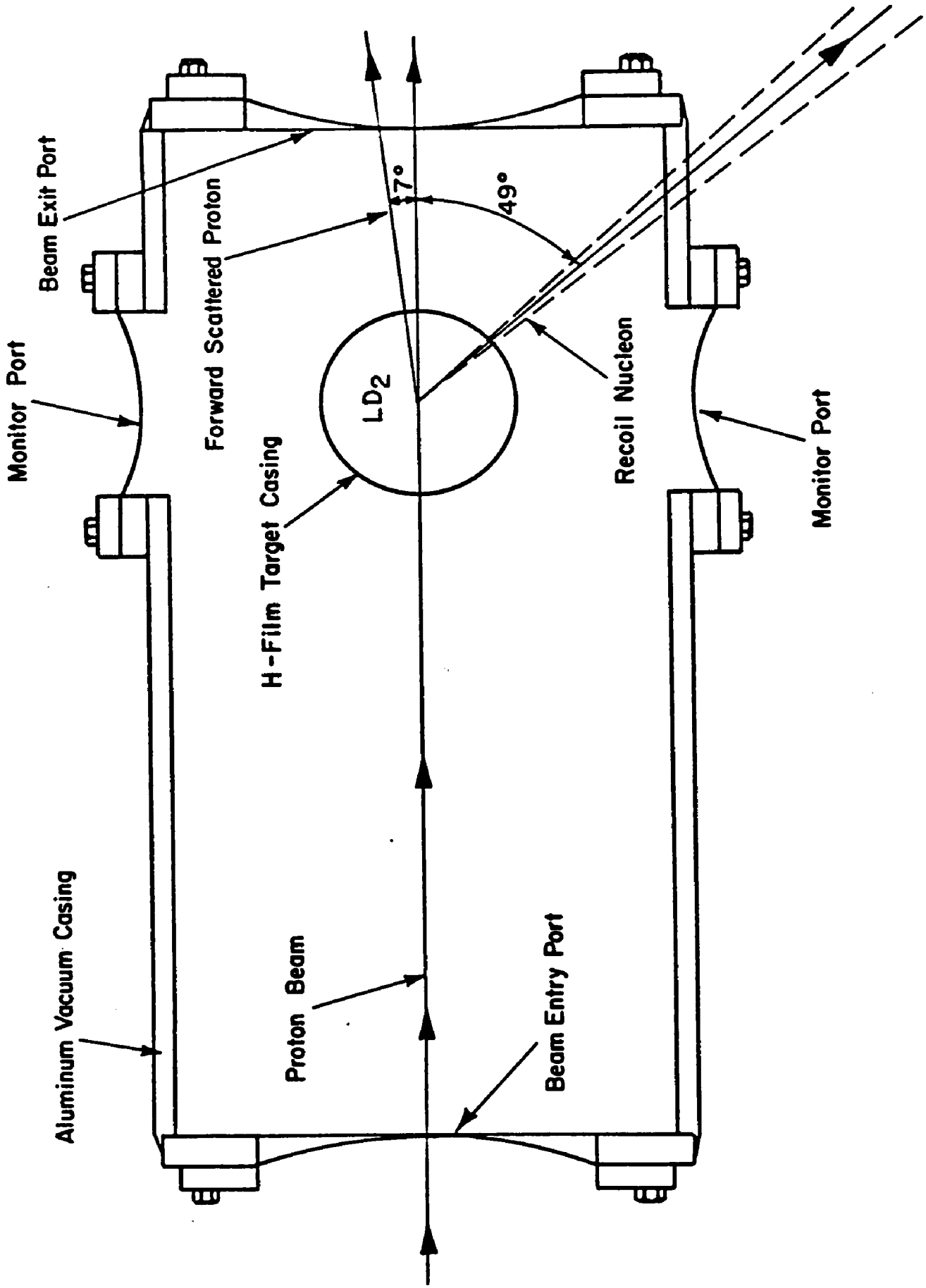

Fig. 3 A top view of the liquid deuterium target and its vacuum casing. Dotted lines indicate solid angle subtended by the sandwich counter.

axis with 0.005 in. H-film windows at each end. The forward proton exited through the downstream window, but the recoil nucleon passed through the aluminum vacuum vessel before reaching the sandwich counter. The ports facing the monitor counters were also covered with 0.005 in. H-film. The target empty counting rate in the spectrometer alone was approximately 25 percent of the target full rate, but the coincidence target empty rate was only one percent of the full rate.

C. Spectrometer and Counters

The spectrometer which detected the forward proton was essentially identical to the one described in greater detail in Ref. 4. The two "B" magnets bent the proton through 5.5^{o} each for momentum analysis. The "C" magnet compensated for different particle scattering angles by steering the desired protons into the spectrometer. For this experiment the forward proton was very close to the 7° central axis of the spectrometer so the "C" magnet was operated at small or zero current. A spectrometer trigger required coincidence of all seven scintillation counters and an anti-coincidence of a nitrogen-filled threshold Cherenkov counter.

The first three scintillation counters, located 60 in. downstream of the first "B" magnet, formed a triple coincidence $S_{123} = S_1 S_2 S_3$. The Cherenkov counter (C_2) was placed in anti-coincidence ($C = C_1 \bar{C}_2 C_3$) with two nearby scintillation counters to eliminate pions or kaons. The two scintillation counters at the end of the spectrometer formed a double coincidence $S_{45} = S_4 S_5$. The coupled momentum

and horizontal scattering angle of the forward proton was defined by S_1 and S_5. S_5 alone defined the vertical acceptance. All other counters were overmatched.

The Pilot B scintillators were coupled to RCA 7746 photomultipliers by air light pipes for the three upstream counters and lucite pipes for the rest. Using air light pipes and placing the lucite pipes at various orientations reduced the coincidence rate due to Cherenkov radiation from particles passing through the light pipes. Light in the 72 in. Cherenkov counter was reflected by a 0.125 in. aluminized lucite mirror through a light pipe into an RCA 8575 photomultiplier. This tube used a bialkalai photocathode to attain high quantum efficiency for low-level Cherenkov light. Voltages for all photomultipliers were determined by running standard plateau curves. The gas pressures for the Cherenkov counter were set after running pressure curves.

D. The Sandwich Counter

The recoil nucleon was detected by the sandwich counter (T counter), which consisted of six 2 in. thicknesses of steel interspersed with six $\frac{1}{2}$ in. Pilot Y scintillation counters. The first two scintillators were 12 in. wide by 9 in. high; the next two were 14 in. by 11 in. and the last two were 15 in. by 12 in. The scintillators were optically connected to RCA 7746 photomultipliers by constant-area lucite light pipes, to maximize light transmission. All the photomultiplier bases had a separate high current supply for the last dynode and a Zener diode on the next-to-last dynode

to eliminate voltage sag at high counting rates. A T counter event occurred whenever there was at least one minimum-ionizing particle in any one of the six scintillation counters.

The photomultiplier voltages for the sandwich counter were set to equalize the output pulse heights for single minimum-ionizing particles. With all steel removed from the counter, high voltage plateau curves were run on one counter in coincidence with two others or with the spectrometer. A spectrometer coincidence indicated that a minimum-ionizing recoil proton from a pp elastic scattering event in the target filled with hydrogen passed through the sandwich counter. This process was iterated until a consistent set of voltage settings emerged.

The sandwich counter was located 156 in. from the target at an angle of 49° from the beam. It was separated from the proton tunnel by an 18 in. steel wall with a hole cut to allow the recoil nucleons to reach the counter.

Directly in front of the sandwich counter, a 15 x 12 x $\frac{1}{4}$ in. scintillation counter was used to determine the charge of the recoil nucleon. Placing this A counter so close to the steel of the sandwich counter complicated the identification of the recoil nucleon. There was the possibility that a neutron could interact in the steel and backscatter a charged particle into the A counter, thus faking the signature of a proton. This ambiguity was corrected by the results of a Monte Carlo calculation, but uncertainties in

the calculation limited the precision of the measurement of the pn to pp scattering ratio. A high current supply and Zener diodes were also used for this counter to eliminate voltage sag at counting rates in excess of 1 Mhz.

The relative efficiencies and solid angles for detecting protons and neutrons were calculated for the sandwich counter using a Monte Carlo simulation of the nuclear cascade, which is described in detail in Ref. 7. The counter detected a proton if it or its reaction products passed through two inches of steel and reached the first scintillator. It detected a neutron only by production of charged secondaries which passed through one of the scintillation counters. The detection of neutrons near the edges of the counter was also hampered by the possibility that all charged reaction products might scatter outside the sensitive volume.

The Monte Carlo simulation followed the general method of earlier calculations for shielding purposes[8]. As the incident nucleon and its reaction products passed through the counter, they were subject to elastic and inelastic scattering in accordance with the probabilities given by Ranft[8]. The momentum and angular distributions for the scattered particles after an inelastic collision were computed according to commonly-used fits to particle production spectra[8]. The types of particles produced were determined by experimental multiplicities for this momentum region[9] and the number of particles produced was set by the requirement of conservation of energy. Since most quasi-elastic scattering

involves a small momentum transfer, the recoil particle for this process was ignored. Ionization and multiple Coulomb scattering were calculated for charged particles. Neutral pion decay into two gammas was considered and the probability of gamma conversion was interpolated from the results of Monte Carlo calculations of the electromagnetic cascade[10]. For simplicity, charged pion decay was ignored.

The reliability of the Monte Carlo model was determined by two different methods. The validity of the assumptions concerning the nuclear cascade were tested by calculating the ^{18}F activity induced by 1 GeV protons in thin aluminum foils interspersed in a block of steel. The calculated activities were compared with measurements made by Shen[11] for a similar situation as shown in Fig. 4. The second method, which tested both the nuclear and electromagnetic portions of the model, involved calculation of the apparent proton and neutron counting rates for seven different steel configurations of the sandwich counter, including no steel. The coincidence counting rate for both pn and pp events was also experimentally measured for the same steel configurations. The number of events in the spectrometer, which detected the sum of pn and pp scattering independently of the sandwich counter, was used as a monitor for these runs. The coincidence rates displayed the same dependence on steel thickness as the calculated proton and neutron efficiencies, as shown in Fig. 5. By adjusting the normalization of the experimental curves to fit the calculated curves, the

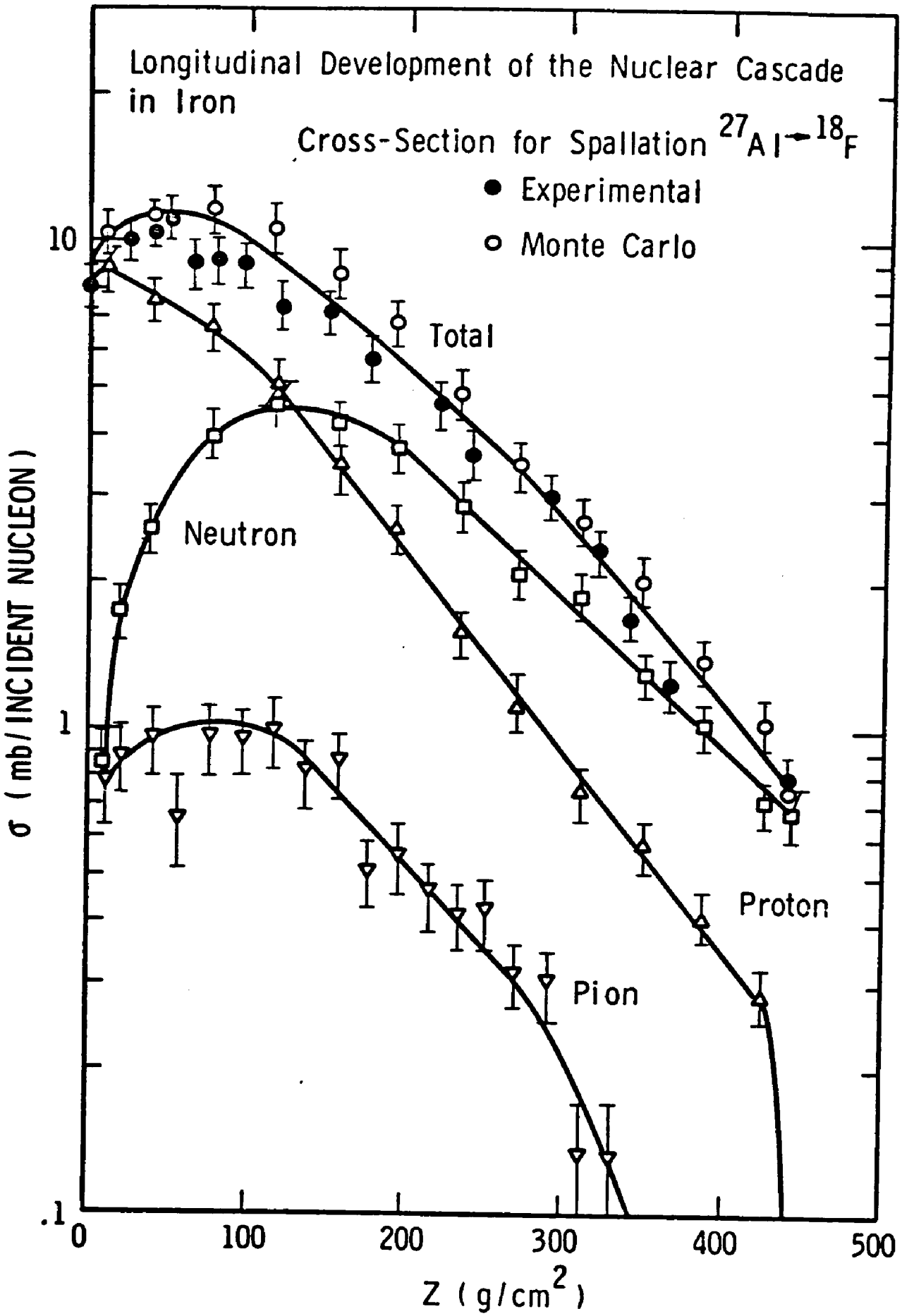

Fig. 4 The longitudinal development of the nuclear cascade from 1 GeV protons in a steel block. Errors shown are statistical only.

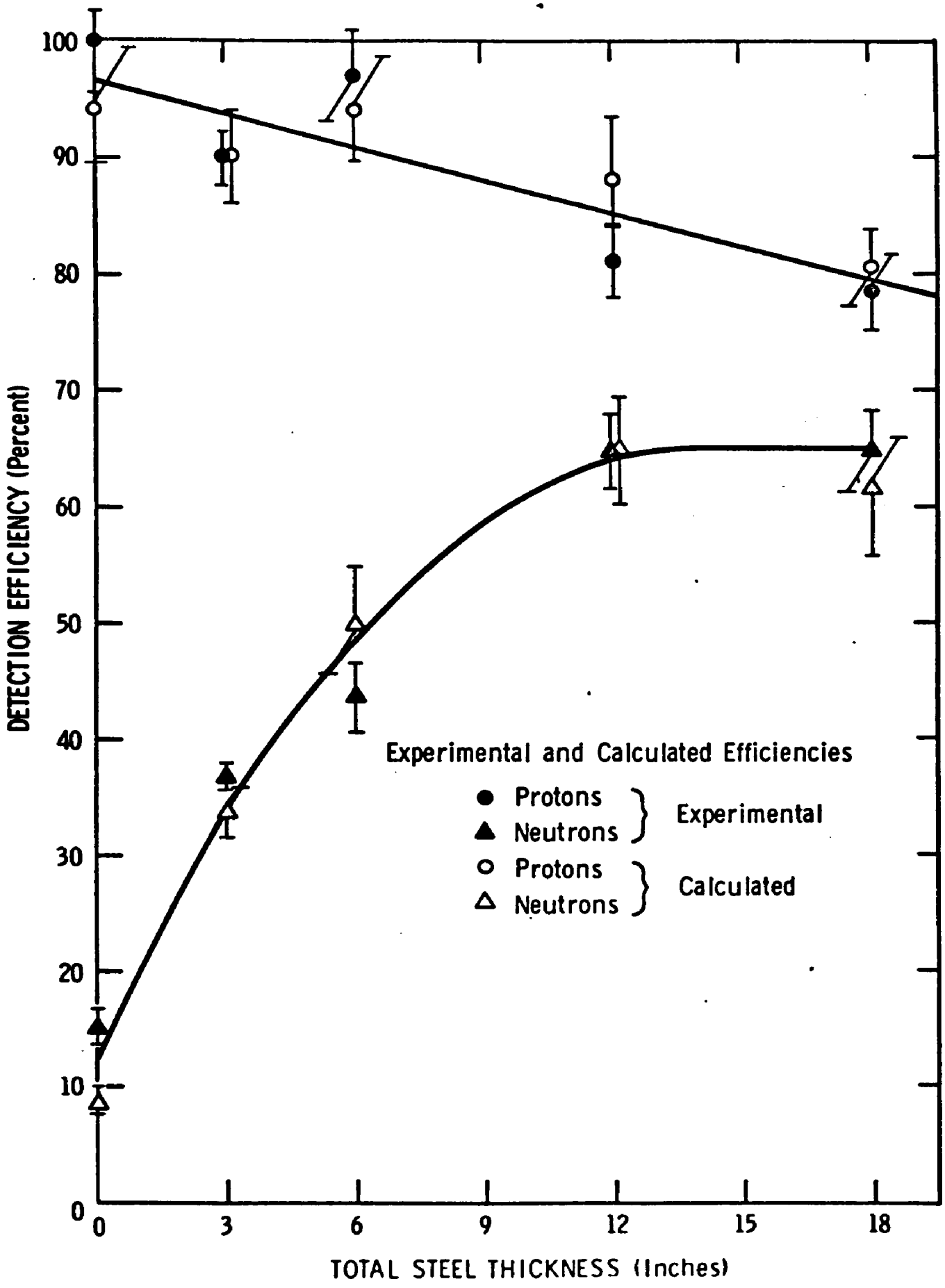

Fig. 5 Comparison of the experimental and calculated counting rates for the sandwich counter with different steel configurations. Recoil nucleon distribution and backscattering effects are included in the calculated rates.

remaining parameter--the ratio of pn to pp scattering--was fixed. The chi-squared confidence level for this fit was larger than 40 percent[12].

The calculated neutron detection efficiency was 75 ± 6 percent at the center of the sandwich counter and dropped toward the edges as shown in Fig. 6. The calculated central detection efficiency for protons was 98 ± 1 percent. The proton efficiency profile is shown in Fig. 7.

The assessment of the given errors in the Monte Carlo calculation followed from a detailed analysis of the various reasons for counter inefficiency. The error in determining that 25 percent of the incident neutrons were not detected could be divided into two parts. Approximately 15 percent of the neutrons passed through the counter without interacting; this number was dependent only on the inelastic cross-section. Knowledge of that cross-section to 10 percent implied only a three percent error in the detection efficiency. This left 10 percent of the incident neutrons which interacted but were not detected because of production of neutrals, absorption of charged secondaries or scattering of secondaries outside the sensitive volume. Assumption of a somewhat arbitrary 50 percent error in the calculation of this process implied a 5 percent error in the overall efficiency. Considering these errors in quadrature resulted in the central detection efficiency uncertainty of 6 percent.

Two other factors were involved in calculating the correction to the data for sandwich counter efficiency. The

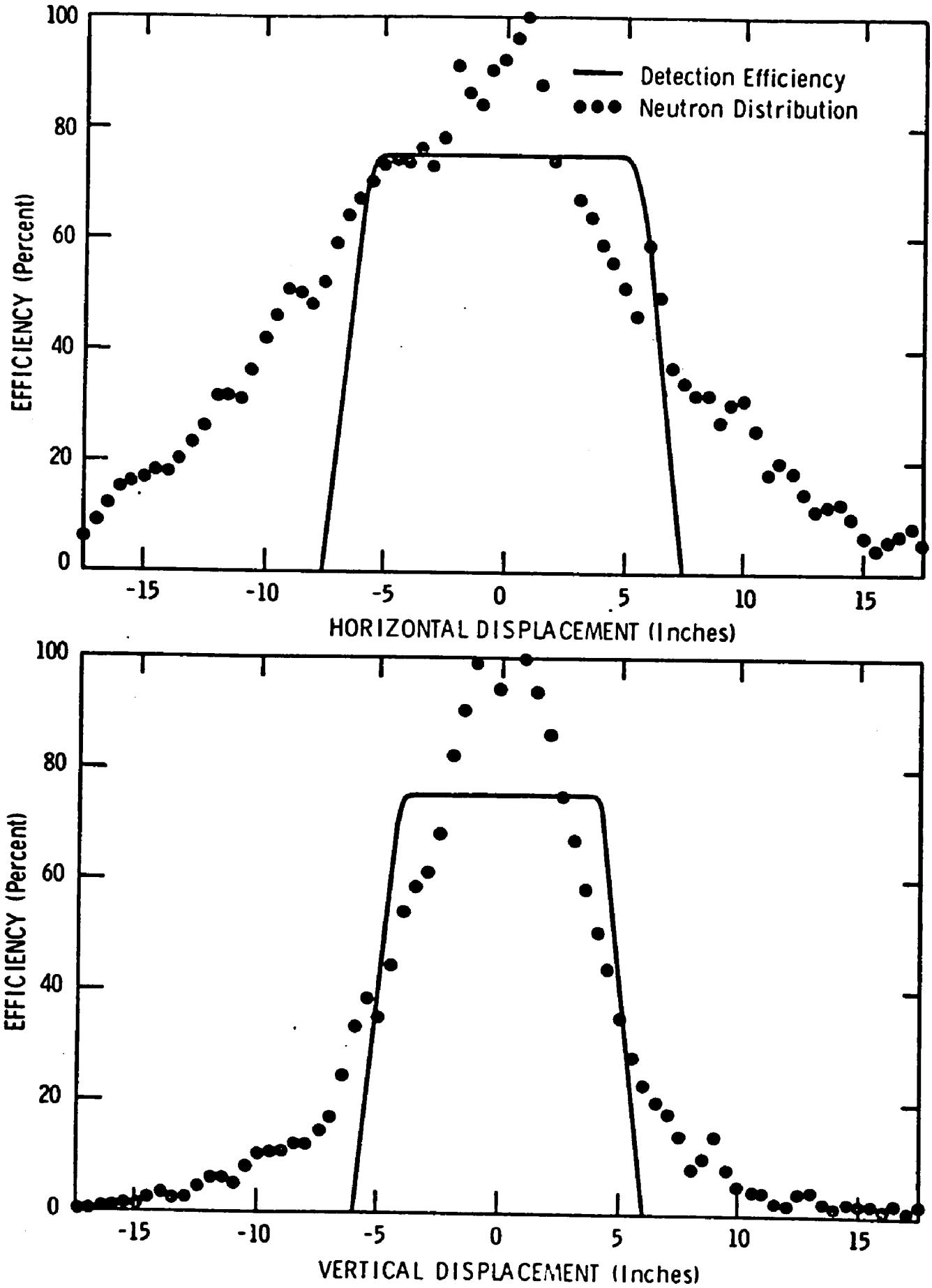

Fig. 6 The calculated sandwich counter detection efficiency for neutrons and the recoil neutron distribution along the horizontal and vertical axes of the sandwich counter.

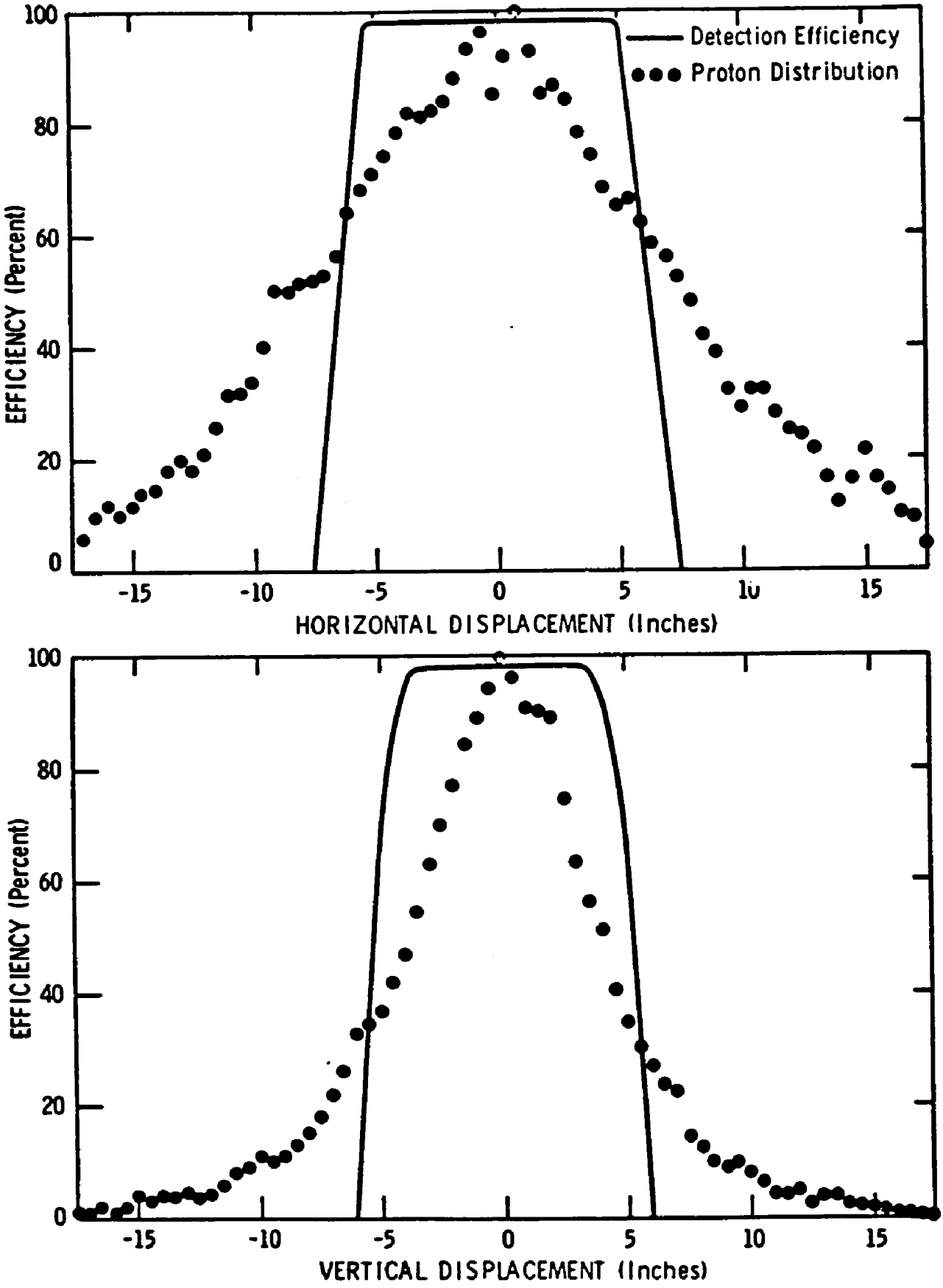

Fig. 7 The calculated sandwich counter detection efficiency for protons and the recoil proton distribution along the horizontal and vertical axes of the counter.

detection function for the counter was weighted by the distribution of recoil nucleons across the face of the counter. This non-uniform distribution was influenced by the Fermi momentum of the target deuteron as well as by the angular divergence and momentum dispersion of the beam, the phase space bite of the spectrometer and the finite size of the target. The calculated horizontal and vertical distributions are shown in Figs. 6 and 7 for the maximum counting rate point. The asymmetry in the horizontal distributions was due to not setting at the exact maximum of the quasi-elastic peak, which resulted from the $\pm\frac{1}{2}$ percent uncertainty in the incident momentum. Scanning across the quasi-elastic peak minimized any uncertainty from this effect in the final cross-section ratio.

The other correction involved the possibility of a charged secondary from an incident neutron backscattering into the A counter. The Monte Carlo simulation calculated that 11.6 ± 4 percent of the recoil neutrons were detected as protons because of backscattering. Approximately half the backscattered charged particles were low energy pions; the remainder were mostly electrons from a converted gamma along with a few protons. The four percent uncertainty includes an estimation of systematic effects, as well as Monte Carlo statistical errors.

E. Electronics

Signals from the photomultipliers were logically analyzed by Chronetics 100 Mhz. circuitry. Compatible TSI

scalers displayed the output of the logic system. A TMC 400-channel pulse height analyzer accumulated and displayed the time-of-flight spectrum between the two detector arms.

The trigger indicating that a proton of the proper momentum passed through the spectrometer was the triple coincidence $SC_{fast} = S_{123}S_{45}C$. As shown in Fig. 8, this signal and the logical OR output of the sandwich counter formed a two-fold coincidence $SCT_{fast} = SC_{fast}T$, which indicated an elastic scattering event. To separate pp elastic from pn elastic events, the SCT_{fast} signal formed both a two-fold coincidence and a two-fold anti-coincidence with the A counter. These outputs were separately scaled as $SCTA_{fast}$ for pp events and $SCT\bar{A}_{fast}$ for pn events.

The high singles rates in both the sandwich and A counters, typically of order 1 Mhz., necessitated the formation of additional coincidences to permit correction for accidentals. A second coincidence, with a resolving time much longer than the first, allowed extrapolation of the coincidence rate to zero resolving time. The outputs of S_{123}, S_{45} and C were stretched by separate discriminators and formed another triple coincidence SC_{slow} with a resolving time of 30 nsec as opposed to 5 nsec for SC_{fast}. The extrapolation method calculated that the number of accidentals in SC_{fast} was $(SC_{slow} - SC_{fast})/ 5$. Similarly, the SC_{slow} output was stretched and formed a two-fold coincidence with T, SCT_{slow} with a resolving time of 60 nsec compared with 7 nsec for the fast coincidence. The SCT_{slow} output formed a fast

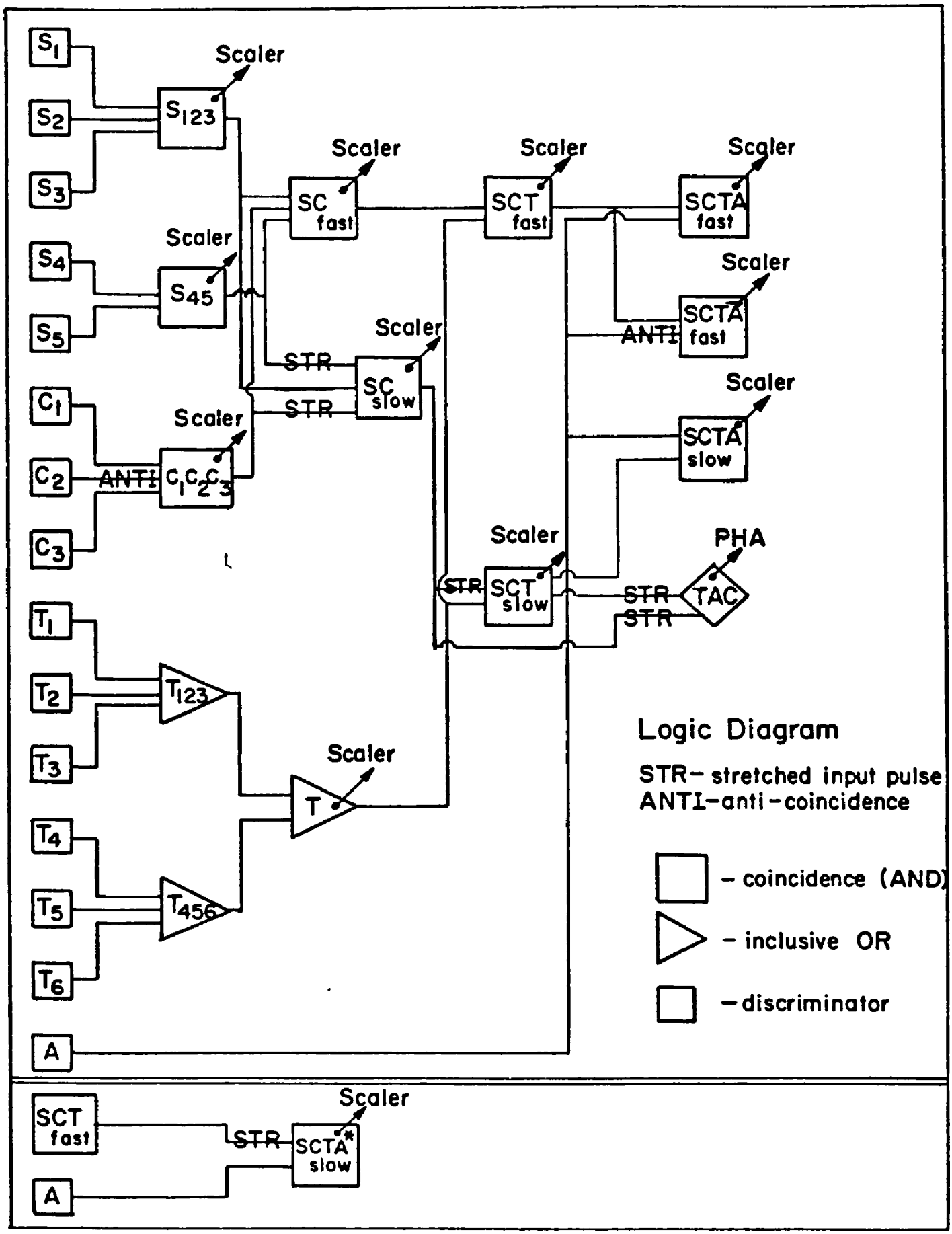

Fig. 8 Block diagram of the logic for the various slow and fast coincidences and the time-of-flight spectrum.

coincidence with A; this coincidence was separately scaled as $SCTA_{slow}$. For some data runs another system of slow coincidences was used. SC_{slow} and SCT_{slow} were formed as before, but the output of SCT_{fast} was stretched in a discriminator and formed a two-fold coincidence with A with a resolving time of 50 nsec which was scaled as $SCTA^{*}_{slow}$. The resolving times for the $SCTA_{fast}$ and $SCT\bar{A}_{fast}$ coincidences were 10 nsec and 5.5 nsec respectively.

The true number of triggers of the type SCTA and $SCT\bar{A}$ was determined by solving a set of five simultaneous linear equations involving SCT_{fast}, SCT_{slow}, $SCTA_{fast}$, $SCTA_{slow}$ and $SCT\bar{A}_{fast}$. Three types of accidental coincidences were considered significant and included in the calculation--an accidental between arms associated with a A count, an accidental between arms not associated with an A count and a true coincidence between arms associated with an accidental A count. The calculation of the five quantities (three types of accidentals and the number of protons and neutrons) from five observables resulted in a no constraint fit. For the second electronics arrangement, which formed $SCTA^{*}_{slow}$, the 5 x 5 accidentals correction matrix was singular and consideration of the two arm accidental associated with an A count was dropped, yielding a non-singular 4 x 4 matrix. This procedure introduced only a small error since this type of accidental was consistently the most infrequent in those data runs for which it could be calculated.

To check the accuracy of the whole system of slow and

fast coincidences, a time-of-flight spectrum between the two arms was accumulated. The timing overlap between two stretched pulses from the SC_{slow} and the SCT_{slow} coincidences was converted to a pulse height by a time-to-amplitude converter (TAC). The TAC output was analyzed by a pulse height analyzer and printed out at the end of each data run as a spectrum with a width of ~2 nsec FWHM. A typical spectrum with a resolution of approximately $\frac{1}{4}$ nsec per channel is shown in Fig. 9.

As indicated in Table 1, the accidentals correction was 3 percent for pp events from hydrogen and 9 percent for pp events from deuterium. There was no net accidentals correction for pn events from deuterium, although the uncertainty in the two offsetting corrections from different types of accidentals resulted in a 4 percent total uncertainty in that result. These two types of accidentals each amounted to approximately 10 percent of the total number of pn events.

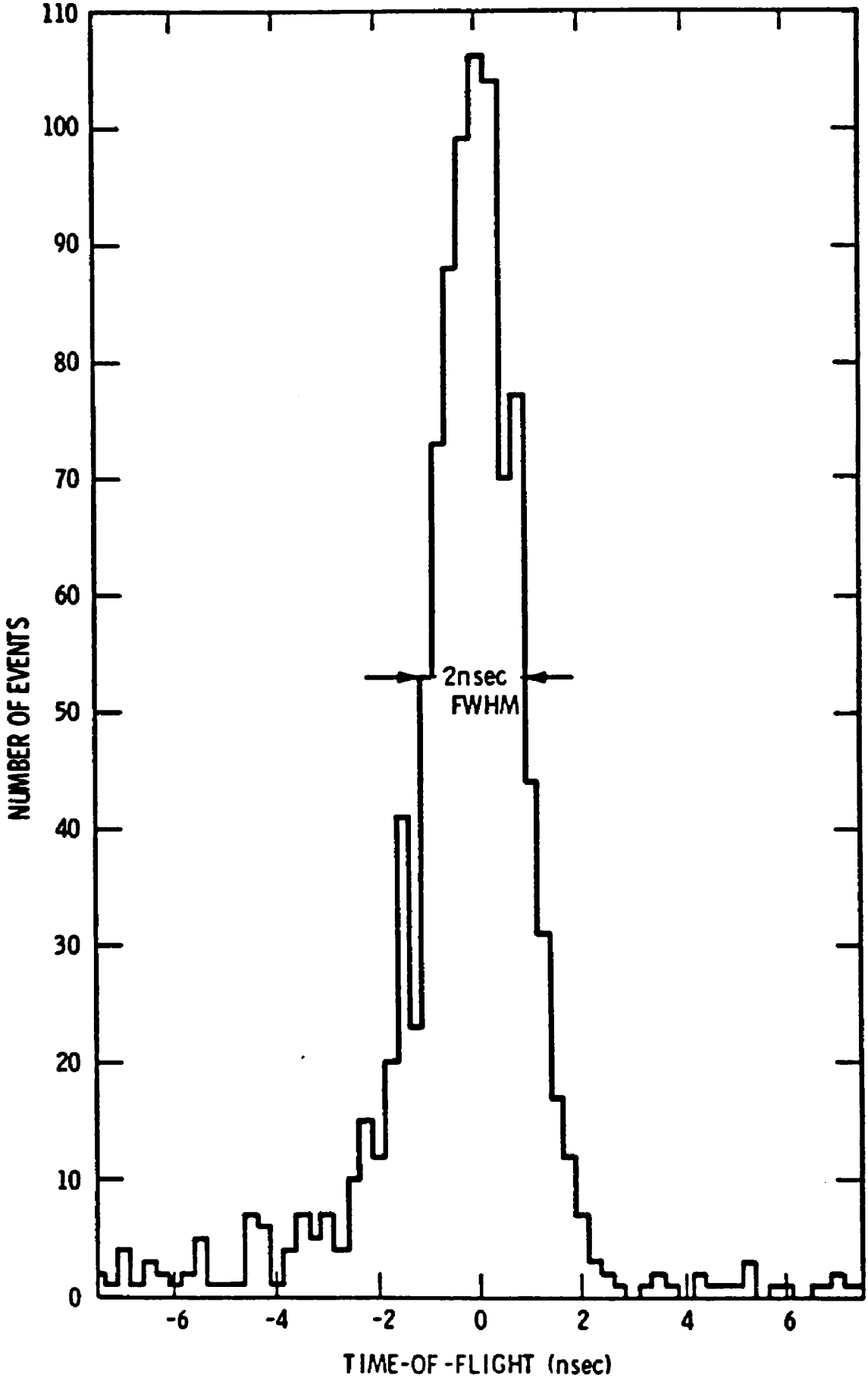

Fig. 9 A typical two arm time-of-flight spectrum with a width of 2 nsec FWHM.

III. RESULTS

A. Corrections and Experimental Errors

The major systematic errors in the experiment arose from an uncertainty in the magnitude of corrections to the raw experimental data. Corrections were made for nuclear absorption, multiple Coulomb scattering, sandwich counter efficiency, backscattering in the sandwich counter, discriminator deadtime, accidental coincidences and target empty counting rate. Data points outside the quasi-elastic peak were used to extrapolate a uniform inelastic background subtraction under the peak. As shown in Table 1, the subtraction was 2.5 percent of the peak for pp scattering and 8 percent for pn scattering. The different subtractions indicated the possibility of additional "noise" in the pn signal because one less coincidence was required ($SCT\bar{A}$ for pn instead of SCTA for pp). The size of the subtraction was consistent with Monte Carlo studies, which showed that only N*(1238) production could result in a large background. Since the N*(1238) cross-section falls quickly with momentum transfer[13], for the point measured the background was small. The phase space for each data point in the scan across the quasi-elastic peak was also calculated by a Monte Carlo program which considered target spot size, angular divergence and chromatic dispersion. The agreement shown in Figs. 10 and 11 between the shape of the experimental quasi-elastic peak and the phase

Table 1
Errors and Corrections

Type	PP Events (Hydrogen)		PP Events (Deuterium)		PN Events (Deuterium)	
	Correction	Error (percent)	Correction	Error (percent)	Correction	Error (percent)
Accidental Coincidences	.97	1	.91	3	1.00	4
Discriminator Deadtime	1.02	1	1.02	1	.98	1
Target Empty Events	.99	0	.99	0	.99	0
Inelastic Events	.975	1	.975	1	.92	3
Absorption						
Spectrometer	1.15	3				
Recoil Particle	1.04	1				
Sandwich Counter						
Backscattering			.92	3	1.12	4
Detection Efficiency	1.02	1	1.02	1	1.33	6
Geometrical Efficiency	1.24	5				
Multiple Coulomb Scattering (recoil proton)	1.02	1	1.02	1		
Monte Carlo Phase Space Calculation (statistical)		3		3		4
Experimental Statistics		4.5		3.2		3.9
Monitoring of Incident Intensity						
Spallation Cross-Section		5				
Relative (point-to-point)		2		2*		

Total: PP Cross-Section from Hydrogen--10%; PN/PP Ratio (Deuterium)--13%; PP (Hydrogen)/PP (Deuterium) Ratio--8%; PN Cross-Section--16%

* Contributes to $PP(H_2)/PP(D_2)$ ratio but not PN/PP ratio.

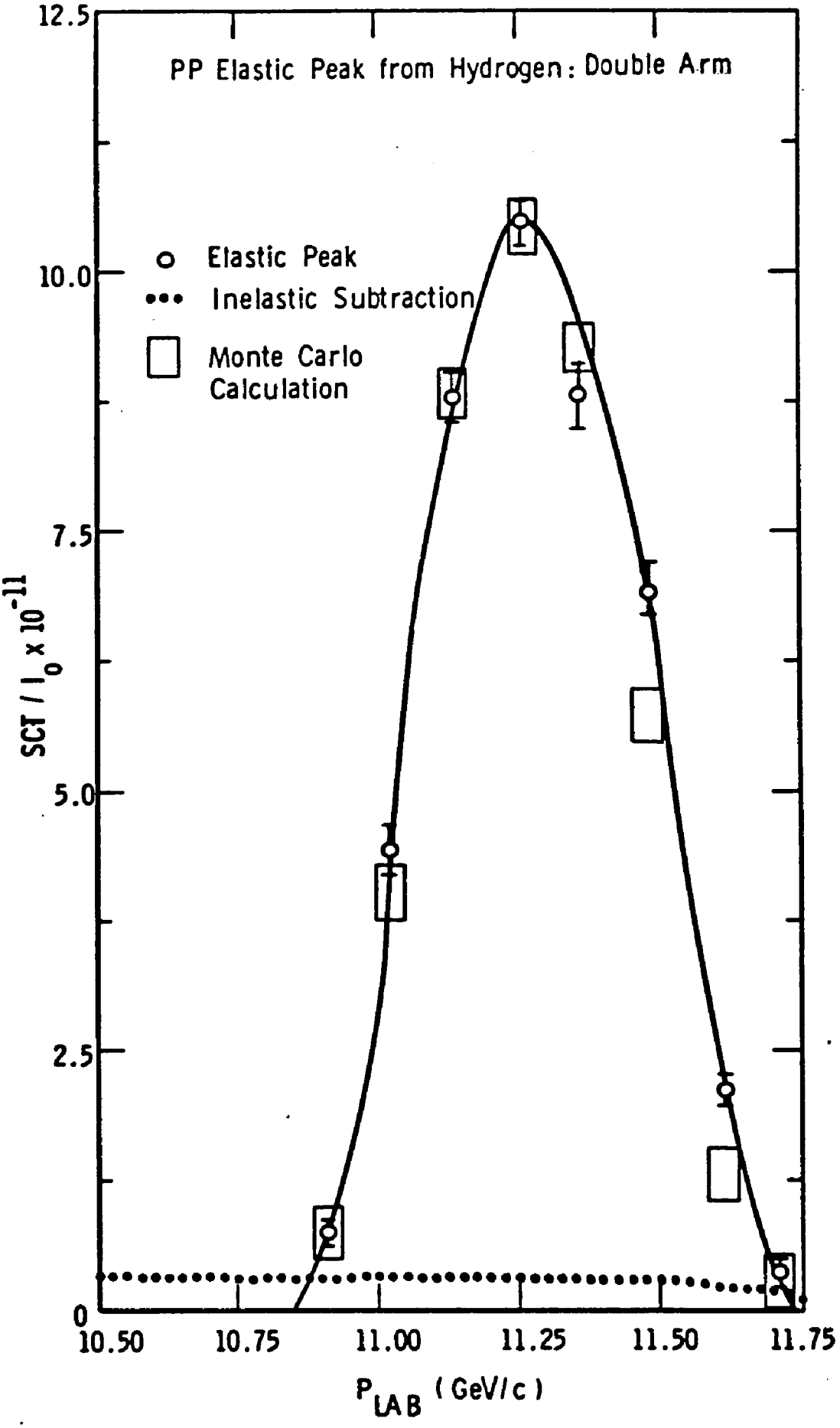

Fig. 10 The pp elastic scattering peak from hydrogen using two arm coincidence data.

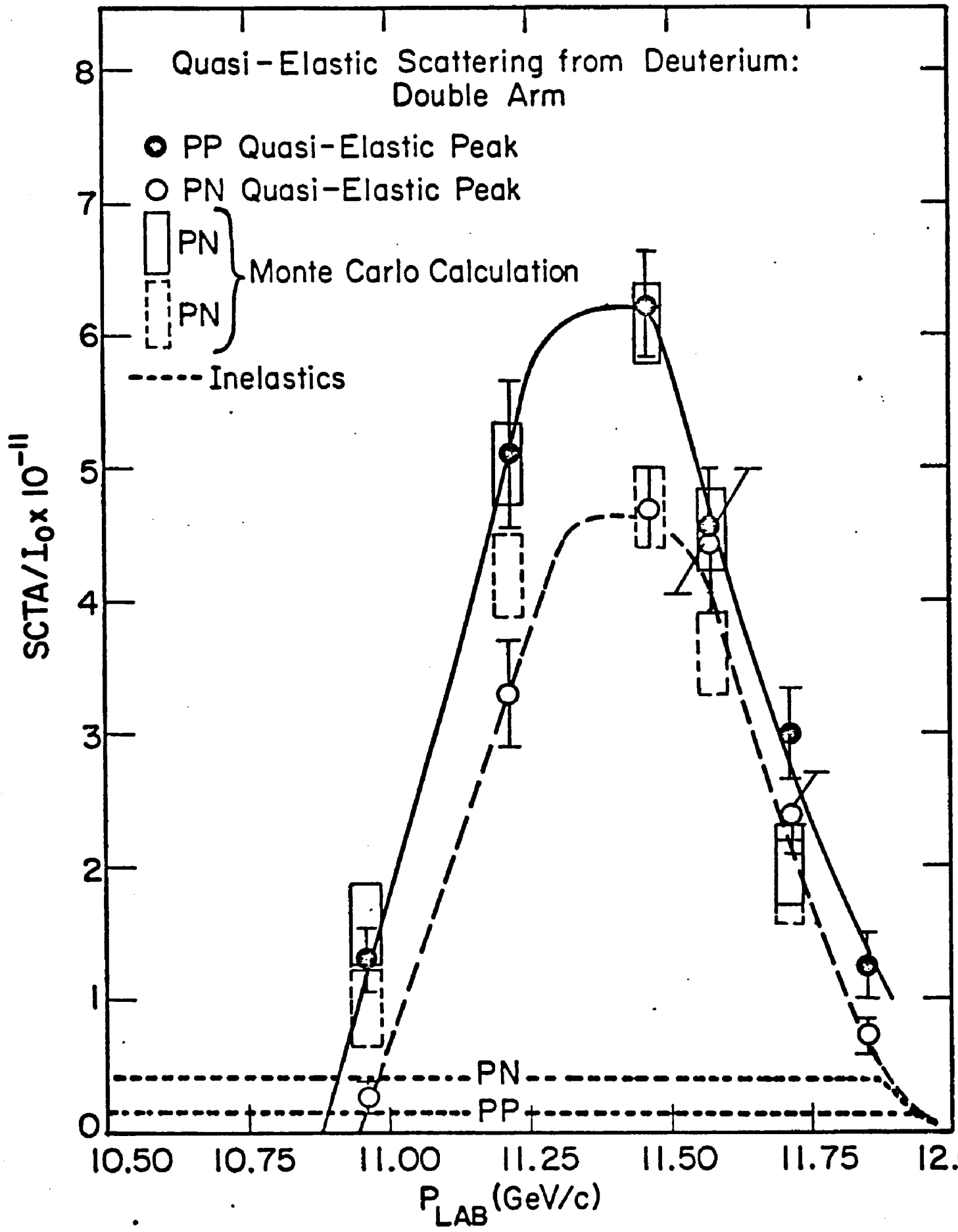

Fig. 11 The pp and pn quasi-elastic peaks from deuterium using two arm coincidence data.

space calculation of the shape confirms the reasonableness of the inelastics subtraction.

Only some of the corrections and their associated systematic errors were applicable to any given datum from the experiment. Nuclear absorption and multiple Coulomb scattering in the spectrometer, for example, affected the absolute pp cross-section but not the pn to pp cross-section ratio. The vast majority of the error in that ratio resulted from uncertainty in the determination of the detection efficiency of the sandwich counter. Table 1 lists the corrections applicable to each of the determined experimental quantities, the amount of the correction and an estimate of the associated systematic error.

The corrections for nuclear absorption were calculated by a Monte Carlo program using appropriate interaction lengths[14] and the same secondary particle spectra as were used for the sandwich counter calibration program. The same Monte Carlo program also determined the multiple Coulomb scattering correction using a Gaussian distribution for the scattering angle. The detailed sandwich counter efficiency profile was folded together with a Monte Carlo calculation of the distribution of recoil nucleons over the face of the counter to determine the correction for sandwich counter inefficiency. The discriminator dead time was taken as twice the duty factor of one percent to compensate for RF structure in the beam. Where comparison was possible, the accidentals subtraction generated by the system of fast and slow coincidences agreed

well within experimental errors with the results of the time-of-flight spectrum. The target empty subtraction was determined by taking otherwise identical data runs with neither hydrogen nor deuterium in the target flask.

B. Proton-Proton Scattering

Proton-proton elastic scattering was measured for the test point of p_o = 12.4 GeV/c, θ^* = 37° using both hydrogen and deuterium targets. Measuring with both targets determined the free pp elastic cross-section--a parameter required in Eq. 2--and permitted a large angle check of the Glauber formalism for multiple scattering[15]. The difference between the elastic pp cross-section from hydrogen and the quasi-elastic pp cross-section from deuterium included the effect of geometrical inefficiency due to the Fermi momentum as well as the multiple scattering defect. To test the Glauber formalism it was necessary to extract the multiple scattering contribution by calculating the effect of geometrical inefficiency. This calculation depended somewhat on the form used for the deuteron wave function. This dependence was not large because only Fermi momenta $\lesssim$ 150 MeV/c were relevant to the calculation. Over this range in momentum space, most proposed wave functions are approximately equal[16]. For the results given here, the Moravcsik fit to the wave function of the Hulthén type[16] was used in the Monte Carlo calculation of the geometrical inefficiency.

The observed free pp cross-section was calculated

according to the equation

$$\frac{d\sigma}{d\Omega} = \left(\frac{1}{N_o \rho t I_o \Delta\Omega}\right)(\text{corrected no. of events}) \quad (3)$$

where N_o is Avogadro's number, ρ is the density of liquid hydrogen (0.07 g/cc), t is the length of the target (2.9 in.), I_o is the incident beam intensity and $\Delta\Omega$ is the solid angle in the center-of-mass. The measured pp center-of-mass cross-section was $\frac{d\sigma}{d\Omega}\Big)_{cm} = 5.8 \pm 0.6$ μb/sr,[17] including a 5.4 percent normalization error, a 4.5 percent statistical error and a 7.2 percent systematic error. The overall cross-section ratio for pp scattering from deuterium to pp scattering from hydrogen was

$$\frac{\text{Deuterium}}{\text{Hydrogen}} = 0.39 \pm 0.03 \quad . \quad (4)$$

After including the results of the calculation of geometrical inefficiency, the ratio due to multiple scattering effects alone was

$$\frac{\text{Deuterium}}{\text{Hydrogen}} = 0.75 \pm 0.09 \quad . \quad (5)$$

The error does not include any uncertainty resultant from the use of an approximation for the deuteron wave function in the geometrical inefficiency calculation.

C. Proton-Neutron Scattering

By the arguments already given, the determination of the pn elastic cross-section is independent of geometrical effects, except for sandwich counter efficiency, and of multiple scattering effects if $R \approx 1$. The measured ratio of

pn scattering to pp scattering, corrected for all experimental effects was

$$R = \frac{\left(\frac{d\sigma}{d\Omega}\right)_{pn}}{\left(\frac{d\sigma}{d\Omega}\right)_{pp}} = 1.05 \pm 0.14 \quad . \qquad (6)$$

The equality of the pn and pp cross-sections makes the consistency argument of Sec. I applicable; the measured pn elastic cross-section at the test point of $p_o = 12.4$ GeV/c and $t' = -2.2$ $(\text{GeV/c})^2$ was then $\left(\frac{d\sigma}{d\Omega}\right)_{cm} = 6.1 \pm 1$ μb/sr or $\frac{d\sigma}{dt} = 3.5 \pm 0.6$ $\mu\text{b}/(\text{GeV/c})^2$.

IV. DISCUSSION

A. Multiple Scattering

The effects of multiple scattering in the deuteron have been explored both theoretically and experimentally in the forward direction[15]. The procedure due to Glauber permits the calculation of the cross-section defect, but simplifying assumptions limit the applicability of the calculation to the high energy, small angle limit. In this limit the predictions of the Glauber model agree well with experimental results. The formalism provides equations for the non-inelastic scattering cross-section and the two-body elastic cross-section. The cross-section for quasi-elastic scattering, which is measured in this experiment, is then

$$\left.\frac{d\sigma}{d\Omega}\right|_{\text{quasi-elastic}} = \left.\frac{d\sigma}{d\Omega}\right|_{\text{non-inelastic}} - \left.\frac{d\sigma}{d\Omega}\right|_{\text{elastic}} \qquad (7)$$

For large momentum transfers, the elastic cross-section is negligible, and the non-inelastic scattering cross-section and the quasi-elastic cross-section are equal.

Analysis of scattering in the forward direction at $t \approx 0$ indicates that the pd elastic process is dominant. The defect in the total pd cross-section at high energies[3] is approximately seven percent, which through the optical theorem implies a 15 percent defect in the elastic differential cross-section. The Glauber equations[15] indicate that at $t \approx 0$ approximately eight percent of the non-inelastic scattering cross-section involves quasi-elastic scattering.

The difference between the non-inelastic differential pd cross-section and the sum of the pp and pn differential elastic cross-sections is about seven percent.

Application of the Glauber formalism to the test point measured in this experiment is complicated by both the small angle and the closure approximations in the model. Closure is assumed in the derivation to permit summation over all allowed proton-neutron final states. The geometry of this experiment does not permit detection of a complete set of proton-neutron final states, so the closure approximation is invalid. It is difficult to determine the error introduced into the final results by these approximations. The Glauber prediction[15] for the ratio of pp scattering from deuterium to pp scattering from hydrogen is

$$\frac{\text{Deuterium}}{\text{Hydrogen}} = 0.85 \qquad (8)$$

using a Gaussian deuteron form factor and Krisch's form for the nucleon-nucleon scattering amplitudes[18]. The measured ratio is 0.75 ± 0.09 indicating no significant disagreement.

The Glauber model, even if it is not particularly applicable, indicates that both the multiple scattering defect and the amount of quasi-elastic scattering relative to two-body elastic scattering increase with increasing momentum transfer. The experimental results confirm this prediction qualitatively and indicate a perhaps greater magnitude than the theory for the multiple scattering defect. Without a detailed, applicable model it is difficult

to determine the complete angular distribution for the multiple scattering defect from the two experimental points at $\theta^* = 0^\circ$ and 37°. The only other available data shows the same trend but is at 1.69 GeV/c incident proton momentum[19].

B. Neutron-Proton Elastic Scattering

The neutron-proton elastic differential cross-section is plotted in Fig. 12 as a function of $\beta_{cm}^2 p_\perp^2$, the variable used by Krisch for an energy-independent plot of all high energy pp elastic scattering data[18]. All of the available large momentum transfer data and a representative sample of the small momentum transfer data is included in the plot[2]. The Krisch variable seems to account for the shrinkage of the diffraction peak for np scattering as well as it does for pp scattering, although the large experimental error bars inhibit a highly constrained fit to a straight line. The slope of the diffraction peak for np scattering is slightly, but significantly, less steep than the slope of the pp diffraction peak--8.5 $(GeV/c)^{-2}$ for np scattering and 10 $(GeV/c)^{-2}$ for pp scattering. In the context of a Lorentz-contracted optical model, the outer radius of the np interaction region is then 0.81 f compared with 0.88 f for the pp interaction[20]. Similar to the pp data, the np cross-section exhibits a "break" at $\beta_{cm}^2 p_\perp^2 = 0.7\ (GeV/c)^2$, although experimental errors prevent a quantitative determination of the slope for the region outside the diffraction peak. There is presently no data at a large enough momentum

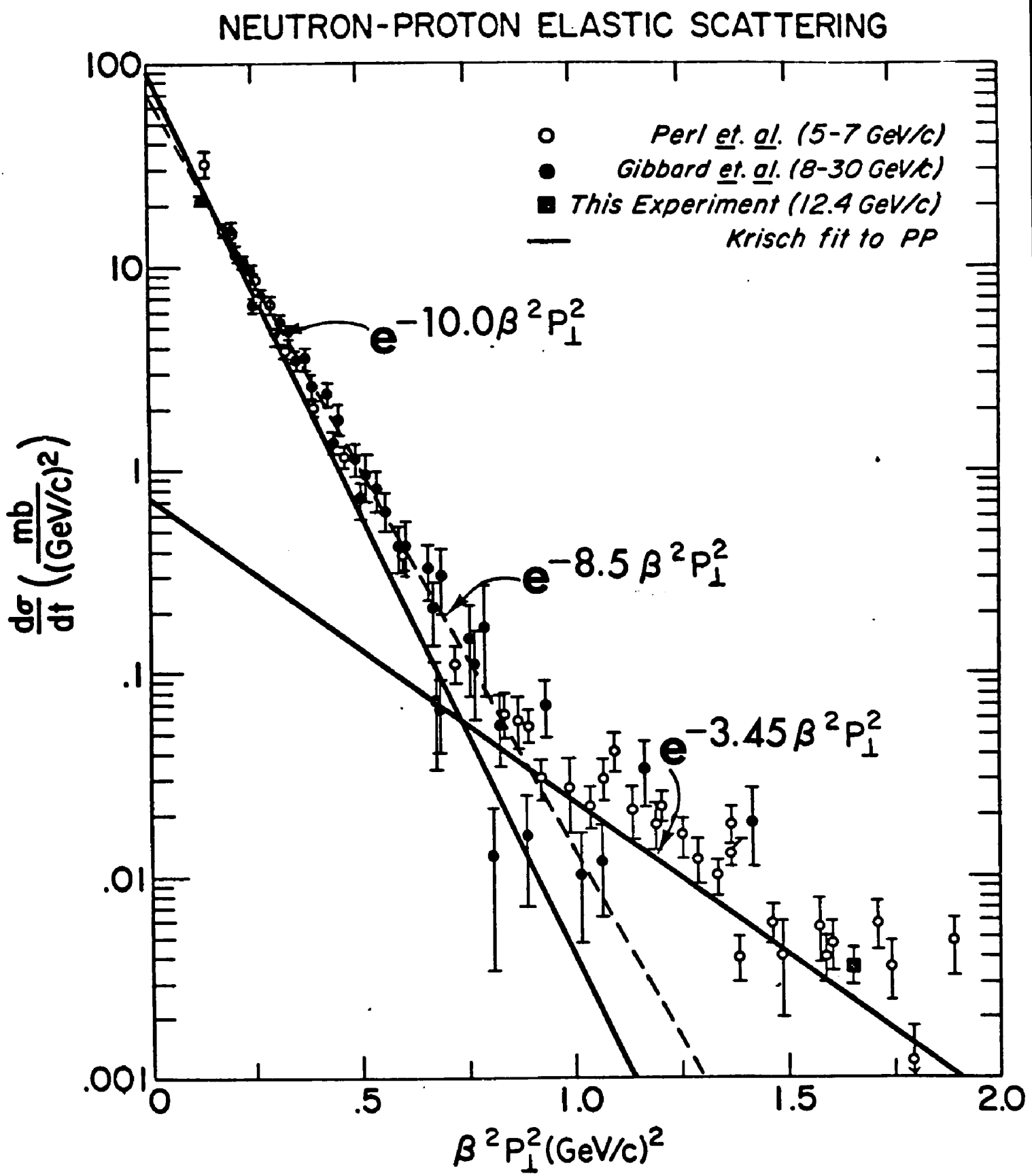

Fig. 12 A plot of np elastic cross-sections as a function of $\beta^2 p_\perp^2$. The solid line is the Krisch fit to the "fundamental" cross-section $\frac{d\sigma^\uparrow}{dt}$.

transfer to indicate whether the np cross-section also follows the second "break" observed in the pp cross-section at $\beta_{cm}^2 p_\perp^2 = 2.8\ (GeV/c)^2$.

The np system is free from particle identity effects which complicate pp scattering near 90° c.m. The data point from this feasibility test and the results of previous experiments indicate that the np and pp cross-sections are approximately equal in the small momentum transfer region. Recent results[2] for incident momenta from 3 to 6 GeV/c indicate that the cross-section ratio at 90° c.m. is given by

$$\left.\frac{np}{pp}\right|_{90^\circ} = 0.63 \pm 0.09 \quad . \qquad (9)$$

This ratio is graphically illustrated in Fig. 12 where the solid line represents the Krisch fit to $\frac{d\sigma}{dt}^\dagger$, which is presumably the "fundamental" pp cross-section independent of particle identity effects[18]. If this model is correct and if the "fundamental" cross-section is independent of nucleon type, then the np data should lie along the line. Because of particle identity effects, the experimental pp cross-section at 90° c.m. is a factor of two above the line, if the interaction is spin-independent.

C. The Deuterium Target Technique

The errors associated with the cross-section measured in this experiment are somewhat smaller than the errors for the neutron beam technique cross-sections of approximately the same magnitude. This comparison indicates that despite some systematic uncertainties, the proton beam-deuterium

target method promises substantially improved measurements of the np elastic cross-section, especially at large transverse momentum.

The errors in this feasibility test can probably be reduced significantly. The largest single uncertainty in the pn/pp ratio is associated with backscattering in the sandwich counter. This correction can be eliminated entirely by moving the A counter far enough from the sandwich counter so that timing discrimination can eliminate false triggers. More extensive experimental measurements of the efficiency of the sandwich counter for neutron detection could eliminate some of the uncertainty which results from imprecise knowledge of the detection efficiency. Time-of-flight spectra on all coincidences would reduce the errors due to accidental coincidences. The use of a hodoscope to provide better resolution of the elastic peak would allow a more careful subtraction of the inelastic background. All these improvements are well-known experimental techniques although they necessarily increase the complexity and cost of the experiment. To measure an angular distribution an additional complication is the necessity for mounting the sandwich counter and its associated shielding on a moveable platform. Implementing all these improvements would reduce the experimental error in the pn/pp ratio from 15 percent to less than seven percent.

A post-experiment review of the three problems anticipated with the deuterium method indicates that they are all

relatively tractable. The smearing effect of the Fermi momentum is unfortunate because it reduces the counting rate, but it can be reasonably well calculated. Indeed as the scattering angle increases, the laboratory momentum of the recoil nucleon increases. Since the angular smearing depends approximately on the ratio p_{Fermi}/p_{recoil}, the smearing and thus the inefficiency become smaller. The loosening of the kinematic constraints on elastic scattering because of the Fermi momentum does not result in an unmanageable inelastic background.

The consistency argument provides a reasonable approach to the problem of multiple scattering in the deuteron if the np and pp cross-sections are approximately equal. That the cross-sections are not equal over the entire angular range seems likely from both experimental data and theoretical considerations. At 90° c.m., the Pauli principle forces inequality unless the nucleon-nucleon scattering amplitudes have a very particular helicity structure. If $R \neq 1$, the effects of multiple scattering at large momentum transfers are not determinable from present theoretical models. Fortunately for the proton beam-deuterium target method, the cross-section ratio seems to differ from unity only near 90° c.m. For large angle scattering, the difference between the quasi-elastic pp cross-section and the elastic pp cross-section is smaller than at small angles where elastic pd scattering dominates. The smaller the difference between the quasi-elastic and elastic cross-sections and

the smaller the difference from unity of the pn to pp cross-section ratio, the smaller the uncertainty in the final result attributable to multiple scattering effects.

The sandwich counter seems a reasonable solution for neutron detection. To allow higher beam intensities which will permit measurements of considerably smaller cross-sections, have investigated by Monte Carlo methods alternate triggering schemes for the sandwich counter which would considerably reduce the counter singles rates. Such schemes seem feasible particularly for the higher momentum recoil neutrons which are produced from interactions at larger scattering angles or higher incident momenta. One possibility would be to require two adjacent scintillators to count instead of any one scintillator. This trigger would place a range requirement on the charged secondaries and therefore set a low energy cut-off on the particles detected.

The most interesting experiment would be to investigate the ratio of pn to pp scattering over the full angular range. The presently poor understanding of the multiple scattering correction at 90° c.m. would partially impair the credibility of some of the results, but since there is no large angle data above 7 GeV/c, all of the data would be useful. There is the additional prospect that this data would help unravel the structure of multiple scattering processes at large momentum transfers. With a higher energy beam, the pd method could determine the existence of a second "break" in the np scattering cross-section, avoiding

completely the 90° c.m. problem. In any event, direct measurement of the pn to pp scattering ratio should reveal considerable information about the spin and isospin structure of nucleon-nucleon scattering.

REFERENCES

1. G. Cocconi, V. T. Cocconi, A. D. Krisch, J. Orear, R. Rubinstein, D. B. Scarl, W. F. Baker, E. W. Jenkins, A. L. Read, B. T. Ulrich, Phys. Rev. 138, B165 (1965). J. V. Allaby, G. Bellettini, G. Cocconi, M. L. Good, A. N. Diddens, G. Matthiae, E. S. Sacharidis, A. Silverman, A. M. Wetherall, Phys. Letters 25B, 156 (1967).
2. M. L. Perl, J. Cox, M. J. Longo, M. N. Kreisler, Phys. Rev. D, (to be published). B. G. Gibbard, L. W. Jones, M. J. Longo, J. R. O'Fallon, J. Cox, M. L. Perl, W. T. Toner, M. N. Kreisler, Phys. Rev. Letters 24, 22 (1970). J. Engler, K. Horn, J. Konig, F. Monnig, P. Schludecker, H. Schopper, P. Sievers, H. Ullrich, K. Runge, Phys. Letters 29B, 321 (1969).
3. W. Galbraith, E. Jenkins, T. Kycia, B. Leontic, R. Phillips, A. Read, Phys. Rev. 138, B913 (1965).
4. J. L. Day, N. P. Johnson, A. D. Krisch, M. L. Marshak, J. K. Randolph, P. Schmueser, G. J. Marmer, L. G. Ratner, Phys. Rev. Letters 23, 1055 (1969). J. L. Day, Thesis, Univ. of Michigan, 1970 (unpublished).
5. F. Hornstra, Jr. and J. R. Simanton, Nucl. Inst. and Meth. 68, 138 (1969). J. R. Simanton, R. F. Margnardt, F. Hornstra, Jr., Nucl. Inst. and Meth. 68, 209 (1969).
6. F. Hornstra, Jr., ZGS Report QR 68-2, Oct. 1968.
7. See Appendix to this thesis.

8. J. Ranft, Nucl. Inst. and Meth. 48, 133 (1967).
T. W. Armstrong and R. G. Alsmiller, Jr. Nucl. Sci. and Eng. 33, 291 (1968).
9. V. S. Barashenkov, V. M. Maltsev, I. Patera, V. D. Toneev, Fortschr. der Physik 14, 357 (1966).
10. D. F. Crawford and H. Messel, Nucl. Phys. 61, 145 (1965).
11. S. P. Shen, BNL-8721 (1964).
12. In calculating the chi-squared the no-steel point for neutrons was ignored. This procedure was reasonable since the predictions of a model based on neutron-steel interactions could not be relevant when only neutron-scintillator interactions could occur.
13. C. M. Ankenbrandt, A. R. Clark, Bruce Cork, T. Elioff, L. T. Kerth, W. A. Wenzel, Phys. Rev. 170, 1223 (1968).
14. N. Barash-Schmidt, A. Barbaro-Galtieri, L. R. Price, M. Roos, A. H. Rosenfeld, P. Soding, C. G. Wohl, UCRL-8030, Jan. 1969.
15. V. Franco and R. J. Glauber, Phys. Rev. 142, 1195 (1966). J. V. Allaby, A. N. Diddens, R. J. Glauber, A. Klovning, O. Kofoed-Hansen, E. J. Sacharidis, K. Schlüpmann, A. M. Thorndike, A. M. Wetherall, Phys. Letters 30B, 549 (1969).
16. M. J. Moravcsik, Nucl. Phys. 7, 113 (1958).
17. This pp cross-section agrees well with nearby measurements done at CERN. See J. V. Allaby, A. N. Diddens, A. Klovning, E. Lillethun, E. J. Sacharidis, K. Schlüpman, A. M. Wetherell, Phys. Letters 27B, 49 (1968).

18. A. D. Krisch, Phys. Rev. Letters 19, 1149 (1967).

19. A. T. Murray, L. Riddiford, G. H. Grayer, T. W. Jones, Y. Tanimura, Nuovo Cimento 49A, 261 (1967).

20. A. D. Krisch, in Lectures in Theoretical Physics, edited by W. E. Britten, et al. (University of Colorado Press, Boulder, 1966) Vol. IX.

APPENDIX

The detection of high energy neutrons by a method which is simultaneously simple and highly efficient (with known efficiency) has proven difficult. In a recent experiment at the Argonne ZGS[1], we have measured the ratio of proton-neutron to proton-proton elastic scattering, using a proton beam and a deuterium target. The forward scattered protons were detected by a 35 m magnetic spectrometer; both recoil neutrons and protons were detected by a steel-scintillator sandwich counter. The sandwich counter inexpensively fulfilled the experimental requirements for an efficient and well-calibrated detector of neutrons and protons. To first approximation the efficiency for protons was 100 percent and for neutrons the efficiency was simply governed by the number of interaction lengths in the counter. Indeed, as the amount of material in the counter increased, knowing the precise number of interaction lengths became less important.

In other experiments the best calibration of detection efficiency has been attained with large-volume scintillation counters, both liquid and solid[2,3]. Yet these counters had a low total detection probability and the large amount of scintillator required was expensive. When precise resolution of the neutron trajectory was necessary, thick plate optical spark chambers were used[4-6], but these chambers sacrificed simplicity and the possibility of "on-line" analysis. Thick plate wire chambers could not be easily utilized since the

many tracks from an inelastic interaction in the plates tended to swamp both the digital readout circuitry and the computer track reconstruction programs. For ultra-high energy cosmic rays[7,8], total absorption ionization calorimeters, which depend on the development of an electromagnetic cascade, could be used both to detect neutrons and to provide crude energy resolution. For incident neutrons with momenta of only a few GeV/c, total absorption counters have proven unsuitable because the electromagnetic cascade does not dominate the energy deposition process.

The steel-scintillator sandwich counter, used in this experiment, was based primarily on the nucleon-meson cascade, rather than the electromagnetic shower used by the calorimeter. Previous experiments with sandwich counters[9,10] have utilized first-order, intuitive ideas about the detection efficiency. To test the applicability of these concepts, we used a series of measurements to validate a Monte Carlo computer simulation of the sandwich counter. The computer program then calculated the detailed efficiency functions required in the experiment.

A. The Sandwich Counter

The physical configuration of the counter in a side view is shown in Fig. 2. Six one-half inch Pilot Y scintillators were interspersed among sets of steel plates 15 in. wide by 12 in. high. The first two scintillators were 12 in. by 9 in., the next two were 14 in. by 11 in. and the back two were 15 in. by 12 in. The nominal center-to-center

separation between scintillators was 4 in. The thickness of steel between any two scintillators was adjustable from 0 to 3 in. in $\frac{1}{4}$ in. increments.

Attached to the front of the sandwich counter was the A counter, a 15 x 12 x $\frac{1}{4}$ in. scintillator, which determined the charge of the incident nucleon. Placing the A counter so close to the steel of the sandwich counter confused the identification of protons and neutrons. A neutron could interact in the steel, backscatter charged secondaries into the A counter and forward scatter secondaries into the sandwich counter, thus faking the signature of a proton. Moving the A counter a few feet from the steel of the sandwich counter would eliminate this ambiguity, because the timing would no longer be identical for neutrons with backscattering and true protons incident on the counter.

The six scintillators of the sandwich counter were each optically connected through a constant-area lucite light pipe, which minimized losses, to an RCA 7746 photomultiplier. The A counter used a similar light pipe attached to an Amperex 56UVP phototube. All photomultiplier bases shared a high current supply for the last dynode and used Zener diodes on the next-to-last dynode to eliminate voltage sag at counting rates up to 1 Mhz.

The photomultiplier voltages were set to equalize the output pulse heights for single minimum-ionizing particles. With all steel removed from the counter, high voltage plateau curves were run on one counter in coincidence with two

others or with the spectrometer. A spectrometer coincidence indicated that a minimum-ionizing recoil proton from a pp elastic scattering passed through the counter. This process was iterated with various counter combinations until a consistent set of voltage settings emerged. Another method used a linear gate and a pulse height analyzer to directly equalize the output pulse heights from the six phototubes. The opening of the gate was triggered by a spectrometer coincidence. The settings from these two methods were essentially identical.

When used to detect neutrons, the outputs from the six photomultipliers were each fed into separate Chronetics 100 Mhz discriminators. The discriminator outputs were folded together by two-stage logical OR circuitry, which provided a sandwich counter output if a minimum-ionizing particle passed through any one of the scintillators.

In operation the sandwich counter was placed 156 in. from a 3 in. liquid deuterium target in the new second extracted proton beam of the ZGS. The counter axis made an angle of 49° to the beam. The counter was separated from the proton tunnel by an 18 in. steel wall with a hole cut to allow the nucleons to reach it. For 10^{10} protons per pulse, the A counter singles rate and the sandwich counter OR counting rate were both of order 5×10^{5} during the 550 msec spill.

B. The Monte Carlo Simulation

The detailed calibration of the sandwich counter was accomplished by a Monte Carlo simulation of the nuclear

cascade; the validity of the calculation was tested by experimentally determining the proton and neutron counting rates for seven steel configurations. Since the counter depended on inelastic interactions it was not perfectly efficient nor was its efficiency constant over its entire active area. The detection efficiency profile of the counter was also, in general, dependent on the momentum of the incident nucleon.

The nuclear cascade model was based on previous calculations[11,12] made to determine adequate accelerator shielding thicknesses. The incident particle and all subsequently produced particles were followed until their momentum was less than 10 MeV/c, although the model was inaccurate at such low momenta since nuclear reactions were not included. The major mechanism considered was inelastic scattering. The parameters which govern these interactions in steel, including the cross-section and the momentum and angular distributions of the produced particles, were identical to those used by Ranft[11]. For inelastic scattering in air and scintillator, the interaction length used was the one published in standard tables[13]. The momentum and angular distributions for steel interactions were also used for scattering in air and scintillator. Because most of the inelastic scattering took place in the steel, this simplification introduced a negligible error. The distribution of types of particles produced was set by multiplicities taken from experimental data in the

1 GeV/c region[14]. The assumption that neutron production from a complex nucleus equaled proton production and that π^0 production equaled π^+ production was used to determine unobserved multiplicities. The total number of particles produced in each interaction was governed by the requirement that the kinetic energy be conserved.

The results of the Monte Carlo simulation were generally insensitive to small changes in the inelastic scattering parameters. The only parameter with a significant influence on the final result was the inelastic cross-section which affected the efficiency in the expected exponential manner. The results of the model were insensitive to raising the low momentum cut-off from 10 MeV/c to 50 MeV/c, to changing all the momentum and angular spectra parameters by 25 percent and to varying the relative multiplicities of nucleons and pions by 25 percent.

The possibility of elastic scattering for all particles was also considered using the cross-sections given in Ref. 11. The angular scattering was computed according to the distribution[15] $e^{-10\beta^2 A^{2/3} p_\perp^2}$. The recoil particle was ignored which resulted in a negligible error in the case of true elastic scattering due to the massiveness of the nucleus. Only a small error resulted for quasi-elastic scattering because most such interactions involve a small momentum transfer.

The effect of multiple Coulomb scattering was calculated according to a Gaussian distribution. Ionization

losses were also calculated for charged particles using a three-term empirical fit to published stopping-power tables[16]. The loss calculated for each particle was determined by its velocity and momentum.

The decay of charged pions was not considered, since the small size of the counter made this process relevant for only low energy pions. These particles had a very short range in steel, as did the low energy muons which would result from a decay. The error from neglecting this process was therefore small. The decay of neutral pions into two gammas was calculated and the electromagnetic shower resultant from the gammas was considered. The shower was approximated by a one dimensional model, with the assumption of normal statistics. The mean and variance of the probability of finding a certain number of electrons at a certain depth in radiation lengths were interpolated from the results of Monte Carlo calculations for copper[17]. This treatment of the electromagnetic cascade was simplified but the effect on the final results was small since only about five percent of the neutrons were detected solely by an electromagnetic shower.

The collective reliability of the assumptions about the nuclear cascade was tested by using the Monte Carlo model to simulate an experiment without adjusting any of the model parameters.[18] The program calculated the ^{18}F activity induced by 1 GeV protons in thin aluminum foils placed within a block of steel 1 ft. by 1 ft. in cross-section. This

calculation used detailed single particle spallation cross-sections as a function of kinetic energy, which have been measured for various particles incident on the aluminum[12]. The comparison with experiment as a function of longitudinal depth is shown in Fig. 4.

C. Results

To test the validity of the Monte Carlo model, the overall detection efficiency of the sandwich counter was calculated as a function of the steel configuration. This computation involved several factors--the detection efficiency at the center of the counter, the drop in efficiency near the edges, the distribution of incoming nucleons and the possibility of a backscattering from an incident neutron into the A counter. For simplicity the incoming neutrons were assumed to be uniformly distributed over the counter area with random directions consistent with their coming from a target. To compare with calculated efficiencies, the experimental data were corrected for accidental coincidences; the effect of faked proton triggers due to backscattering into the A counter was also considered. The comparison of calculated and experimental efficiencies as a function of the total amount of steel in the counter is shown in Fig. 5. The normalization between the experimental proton and neutron efficiencies assumed that the ratio of incoming protons to neutrons was 0.95.[1] The lack of agreement at the no steel point for neutrons was not unexpected. A model based on the nuclear cascade in steel should not be able to predict

experimental efficiencies with no steel present. The comparison between calculated and experimental efficiencies for a fixed amount of steel distributed in different amounts between scintillators showed similar agreement.

The Monte Carlo simulation was then used to calculate detailed detection efficiency profiles for the "12 in. total--2 in. between scintillators" steel configuration, which was the arrangement used in the pn scattering experiment. The program was also used to calculate a correction for the misidentification of protons and neutrons resultant from backscattering into the A counter. The high singles rate observed in the sandwich counter motivated the consideration of triggering schemes other than one particle in any one scintillator. Detection efficiencies were also calculated for the trigger requirements "any one counter," "any two counters," "any two adjacent counters," "any three counters" and "at least two ionizing particles detected." Any of these schemes would result in a much lower sandwich counter singles rate. Fig. 13 shows the calculated detection profile for 1.8 GeV/c neutrons incident on the horizontal axis of the counter as a function of displacement from the center for the various detection schemes. The detection efficiency off-axis was well-represented by the equation

$$\text{Efficiency } (x,y) = \frac{\text{Efficiency } (x,y=0) \times \text{Efficiency } (x=0,y)}{\text{Efficiency } (x=0,y=0)} \quad (10)$$

The central detection efficiency as a function of

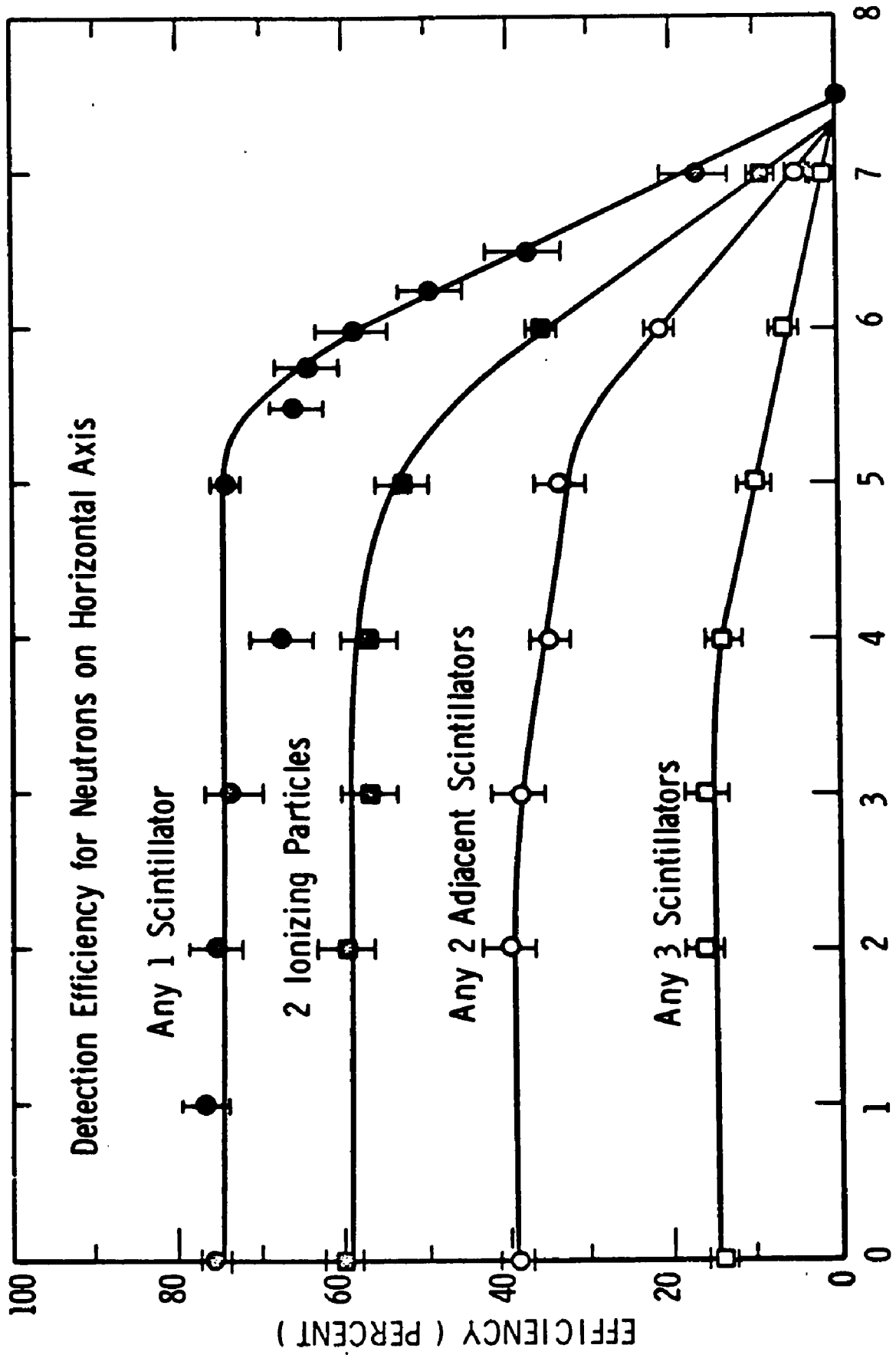

Fig. 13 Detection efficiency for neutrons along the horizontal axis of the sandwich counter for various trigger requirements.

incident neutron momentum for the same "12 in.--2 in." steel arrangement but varying trigger requirements is shown in Fig. 14. The "any one counter" triggering scheme used in the pn experiment had the advantage of a uniform sandwich counter response over a large central area and over the incident momentum range from 1.8 to 5 GeV/c. The non-central detection efficiency profile was also invariant for this triggering scheme over the same momentum range.

To a first approximation then, the detection efficiency for neutrons for the "any one counter" triggering scheme over a large range of incident momenta depended only on two parameters-- the total amount of steel in the counter and the amount of steel between any two scintillators. The inelastic interaction length, which was measured in other experiments as 6.4 in.[11], characterized the probability that a neutron would interact at all in the counter. The other characteristic length was an absorption length which measured the probability that the charged secondaries from a neutron-steel interaction would be absorbed before they could reach a scintillator. From the results of the Monte Carlo calculation, confirmed by experiment, this length was 23 ± 2 in. Thus the detection efficiency over a large part of the counter's sensitive area was approximately

$$\text{Efficiency} = (0.95)\ (1 - e^{-x/6.4})\ (e^{-y/23}) \qquad (11)$$

where x is the total length of steel in inches and y is the amount of steel between any two scintillators. The coefficient 0.95 reflects the probability that a neutron

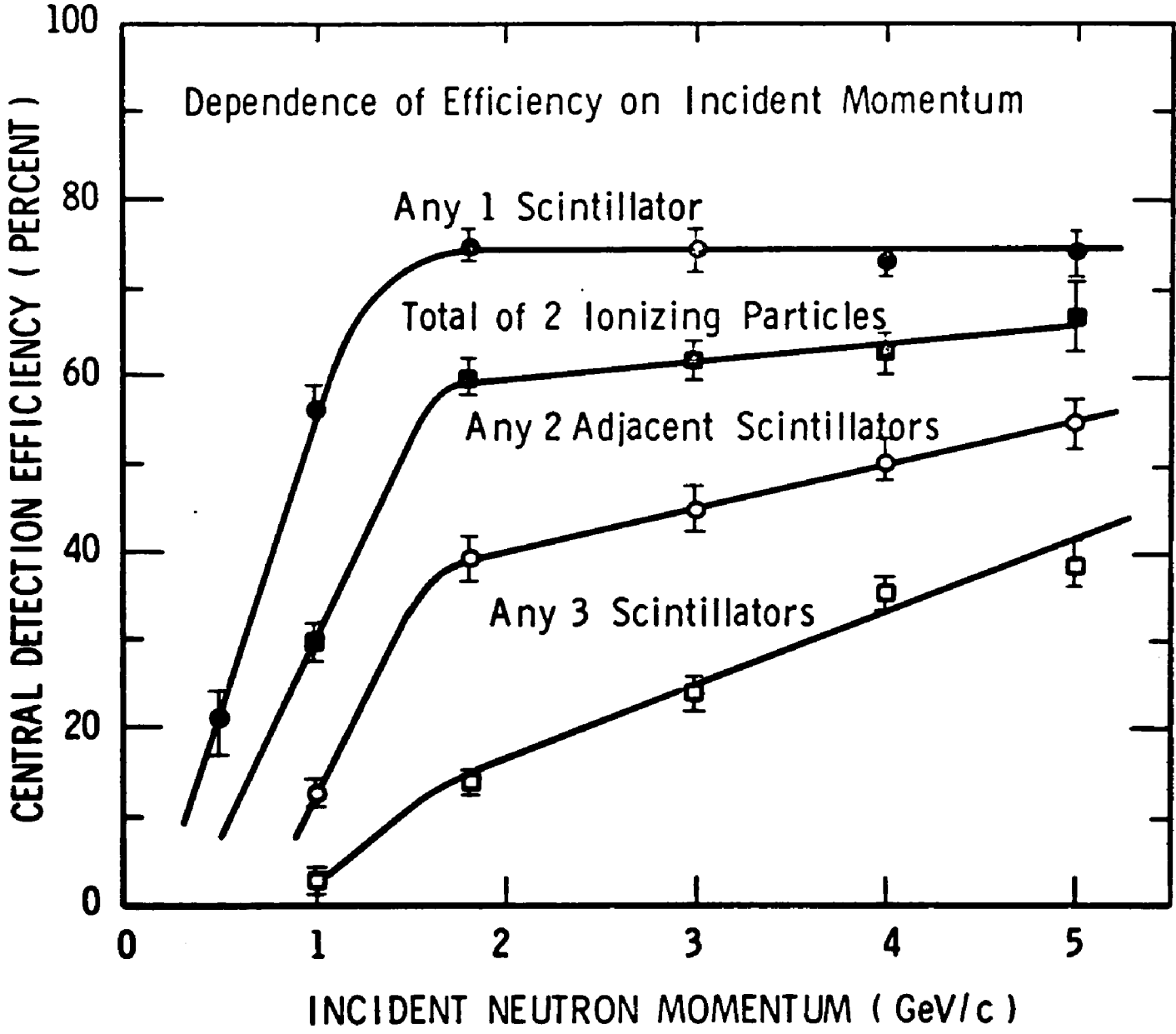

Fig. 14 Sandwich counter central detection efficiency for neutrons as a function of incident neutron momentum for various trigger requirements.

might have interacted to produce only neutrals which were never detected.

The assessment of errors in the Monte Carlo calculation followed from a detailed analysis of the various reasons for counter inefficiency. For the "12 in.--2 in." steel arrangement the computed central detection efficiency was 75 percent, with a two percent statistical error. There were two contributions to the 25 percent loss. Approximately 15 percent of the incident neutrons passed through the counter without interacting; this number depended only on the inelastic cross-section. Knowledge of that cross-section to 10 percent implied only a three percent error in the detection efficiency. This left 10 percent of the incident neutrons which interacted but were not detected because of production of neutrals, absorption of charged secondaries or scattering of secondaries outside the sensitive counter volume. Assuming a somewhat arbitrary 50 percent error in the calculation of this process implied a five percent error in the overall efficiency. Considering all these errors in quadrature resulted in a central detection efficiency for this steel configuration of 75 ± 6 percent.

Determination of the overall sandwich counter response for both types of nucleons involved additional errors. Calculation of "edge effects" and backscattering each introduced an independent four percent error in the calculated counting rates. For comparison with the experimental rates shown in Fig. 5, an additional four percent error

for accidentals correction must be added. Using these estimated errors, the comparisons shown in Fig. 5 yield a chi-squared confidence level in excess of 40 percent for both protons and neutrons, with the exclusion of the no steel point for neutrons.

D. Conclusions

The results of the Monte Carlo calculations corroborate the general validity of the intuitive ideas about the detection efficiency of the sandwich counter. The relatively long length--23 in.--for absorption of secondaries indicates that this is not a serious effect for any reasonable amount of steel between scintillators. The five percent loss in efficiency due to formation of neutrals is relatively independent of the amount of steel. The Monte Carlo calculation also indicates that for the triggering scheme used the detection efficiency for neutrons is relatively constant up to one inch from the edge of the scintillator. The sandwich counter has the considerable advantage that although a judicious mixture of steel and scintillator will optimize its performance for any given momentum particle, to first approximation a straightforward approach is all that is necessary.

REFERENCES

(in the Appendix)

1. See the main text of this thesis.
2. R. Hofstadter, Stanford HEPL Report 599, March 1969.
3. A. S. L. Parsons, P. Trueol, P. A. Berardo, R. P. Haddock, L. Verhey, M. E. Zeller, UCRL-19259, July 1969.
4. R. C. Chase, E. Coleman, H. W. J. Courant, E. Marquit, E. W. Petraske, H. Romer, K. Ruddick, Phys. Rev. Letters, 22, 1137 (1969).
5. M. L. Perl, J. Cox, M. J. Longo, M. N. Kreisler, Phys. Rev. D (to be published).
6. B. G. Gibbard, L. W. Jones, M. J. Longo, J. R. O'Fallon, J. Cox, M. L. Perl, W. T. Toner, M. N. Kreisler, Phys. Rev. Letters 24, 22 (1970).
7. V. S. Murzin, in Progress in Elementary Particle and Cosmic Ray Physics IX, edited by J. G. Wilson and S. A. Wouthhuysen (North-Holland, Amsterdam, 1967).
8. D. E. Lyon and A. Subramanion, Univ. of Michigan preprint, 1967.
9. YU. V. Galaktionov, L. G. Landsberg, V. A. Lyubimov, Nucl. Inst. and Meth. 48, 133 (1967).
10. L. W. Jones, Tech. Report 32, Univ. of Michigan (1968).
11. J. Ranft, Nucl. Inst. and Meth. 48, 133 (1967).
12. T. W. Armstrong and R. G. Alsmiller, Jr. Nucl. Sci. and Eng. 33, 291 (1968).
13. N. Barash-Schmidt, A. Barbaro-Galtieri, L. R. Price, M. Roos, A. H. Rosenfeld, P. Soding, C. G. Wohl, UCRL-8030, Jan. 1969.

14. V. S. Barashenkov, V. M. Maltsev, I. Patera, V. D. Toneev, Fortschr. der Physik 14, 357 (1966).

15. A. D. Krisch, Phys. Rev. Letters 19, 1149 (1967).

16. W. H. Barkas and M. J. Berger, NASA SP-3013,(1964). The empirical fit used was

$$\frac{dE}{dx} = \frac{dE}{dx}\Big)_{min}\left[54.1e^{-9.46/\sqrt{\beta p}} + 6.82e^{-2.13\sqrt{\beta p}}\right] \qquad (12)$$

or $\frac{dE}{dx} = \frac{dE}{dX}\Big)_{min}$, whichever is greater.

17. D. F. Crawford and H. Messel, Nucl. Phys. 61, 145 (1965).

18. S. P. Shen, BNL-8721 (1964).